The hippocampus and medial prefrontal cortex during flexible behavior

by

Karola Kaefer

August, 2019

A thesis presented to the
Graduate School
of the
Institute of Science and Technology Austria, Klosterneuburg, Austria
in partial fulfillment of the requirements
for the degree of
Doctor of Philosophy

The dissertation of Karola Kaefer, titled *"The hippocampus and medial prefrontal cortex during flexible behavior"*, is approved by:

Supervisor: Prof. Jozsef Csicsvari, IST Austria, Klosterneuburg, Austria

Signature:

Committee Member: Prof. Peter Jonas, IST Austria, Klosterneuburg, Austria

Signature:

Committee Member: Prof. Ole Paulsen, Department of Physiology, Development and Neuroscience, University of Cambridge, United Kingdom

Signature:

Exam Chair: Dr. Sandra Siegert, IST Austria, Klosterneuburg, Austria

Signature:

signed page is on file

IST Austria Thesis, ISSN: 2663-337X

I hereby declare that this dissertation is my own work and that it does not contain other people's work without this being so stated; this thesis does not contain my previous work without this being stated, and the bibliography contains all the literature that I used in writing the dissertation.

I declare that this is a true copy of my thesis, including any final revisions, as approved by my thesis committee, and that this thesis had not been submitted for a higher degree to any other university or institution.

I certify that any republication of materials presented in this thesis has been approved by the relevant publishers and co-authors.

Signature: _____

Karola Kaefer

signed page is on file

ABSTRACT

The solving of complex tasks requires the functions of more than one brain area and their interaction. Whilst spatial navigation and memory is dependent on the hippocampus, flexible behavior relies on the medial prefrontal cortex (mPFC). To further examine the roles of the hippocampus and mPFC, we recorded their neural activity during a task that depends on both of these brain regions.

With tetrodes, we recorded the extracellular activity of dorsal hippocampal CA1 (HPC) and mPFC neurons in Long-Evans rats performing a rule-switching task on the plus-maze. The plus-maze task had a spatial component since it required navigation along one of the two start arms and at the maze center a choice between one of the two goal arms. Which goal contained a reward depended on the rule currently in place. After an uncued rule change the animal had to abandon the old strategy and switch to the new rule, testing cognitive flexibility. Investigating the coordination of activity between the HPC and mPFC allows determination during which task stages their interaction is required. Additionally, comparing neural activity patterns in these two brain regions allows delineation of the specialized functions of the HPC and mPFC in this task. We analyzed neural activity in the HPC and mPFC in terms of oscillatory interactions, rule coding and replay.

We found that theta coherence between the HPC and mPFC is increased at the center and goals of the maze, both when the rule was stable or has changed. Similar results were found for locking of HPC and mPFC neurons to HPC theta oscillations. However, no differences in HPC-mPFC theta coordination were observed between the spatially- and cue-guided rule. Phase locking of HPC and mPFC neurons to HPC gamma oscillations was not modulated by maze position or rule type.

We found that the HPC coded for the two different rules with cofiring relationships between cell pairs. However, we could not find conclusive evidence for rule coding in the mPFC.

Spatially-selective firing in the mPFC generalized between the two start and two goal arms. With Bayesian positional decoding, we found that the mPFC reactivated non-local positions during awake immobility periods. Replay of these non-local positions could represent entire behavioral trajectories resembling trajectory replay of the HPC. Furthermore, mPFC trajectory-replay at the goal positively correlated with rule-switching performance. Finally,

HPC and mPFC trajectory replay occurred independently of each other. These results show that the mPFC can replay ordered patterns of activity during awake immobility, possibly underlying its role in flexible behavior.

ABOUT THE AUTHOR

Karola Kaefer started her scientific career in 2007 at the University of Edinburgh where she completed her Bachelor of Science (Hons) degree in Neuroscience. At the laboratory of Prof. Emma Wood she gained first insight into conducting behavioral experiments on rats. In 2011 she then went to the Ludwig-Maximilians University in Munich to pursue a Masters of Science degree in Systemic Neuroscience. There she had the chance to gain experience in several research groups including that of Prof. Mark Huebener at the Max Planck Institute for Neurobiology and that of Prof. Carsten Wotjak at the Max Planck Institute for Psychiatry, where she got familiarized with data analysis. Finally in 2013, she joined IST Austria and a year later the group of Prof. Jozsef Csicsvari, where she worked on two projects. One project focused on hippocampal dysfunctions in a rat model of schizophrenia and the main project investigated neural activity in the hippocampus and medial prefrontal cortex during flexible behavior.

This thesis is dedicated to the memory of my mother.

ACKNOWLEDGEMENTS

Firstly, I want to acknowledge my supervisor Prof. Jozsef Csicsvari for giving me the opportunity to work in his group. Being one of the leading groups that investigate how the brain processes and remembers information, it gave me a thorough background in the current state of the field and the necessary skills to perform research of significance.

I would also like to thank Prof. Peter Jonas and Prof. Ole Paulsen for taking the time to be my thesis committee members and Dr. Sandra Siegert for being the Chair.

During the tgDISC1 project, I closely worked together with Dr. Hugo Malagon-Vina. I therefore want to thank him for guiding me through the first years of my PhD and supporting me with publishing my first paper. I also want to thank Dr. Karel Blahna who I spent many hours in the surgery room with performing the first prefrontal recordings in the group.

I am also very grateful to Michele Nardin who strongly supported me in the analysis of data of the hippocampal-prefrontal project. My programming skills improved significantly due to his patience and teaching skills.

I want to thank all the other members of the Csicsvari group for making the laboratory and office such a pleasant working environment. Special thanks to those that accompanied me through most of my PhD, Dr. Peter Baracskay, Dr. Charlotte Boccara, Dr. Igor Grydchin, Dr. Joe O'Neill, Dama Rangel-Guerrero, Dr. Federico Stella, Jago Wallenschus and Dr. Haibing Xu. Thanks to Uladzislau Barayeu with whom I started working on the theta oscillation analyses. Also, without the drive design and production from Todor Asenov and Thomas Menner the hippocampal-prefrontal recordings would not have been possible.

Last but not least, I want to thank my family. My mother, who was the first to support my wish to pursue Neuroscience in Edinburgh. My father, brother, grandparents and Binder family for their unconditional support throughout the thesis and life in general.

LIST OF PUBLICATIONS DURING PHD THESIS

Original publication

Kaefer, K., Malagon-Vina, H., Dickerson, D. D., O'Neill, J., Trossbach, S. V., Korth, C., Csicsvari, J. Disrupted-in-schizophrenia 1 overexpression disrupts hippocampal coding and oscillatory synchronization. Hippocampus (2019)

Posters and presentations

Kaefer, K. Hippocampal activity in tgDISC1 rats. Neuroscience data talk, IST Austria (2016)

Kaefer, K., Malagon-Vina, H., Dickerson, D. D., O'Neill, J., Trossbach, S. V., Korth, C., Csicsvari, J. Altered hippocampal coding from misassembly of full-length DISC1 protein. Society for Neuroscience abstracts (12.-16. November 2016, San Diego)

Kaefer, K. Replay of trajectories in the hippocampus and medial prefrontal cortex. Neuroscience data talk, IST Austria (2019)

Kaefer, K. Replay of trajectories in the medial prefrontal cortex. Hippocampal research conference (2.-7. June 2019, Taormina)

TABLE OF CONTENTS

LIST OF FIGURES **12**

ABBREVIATIONS **13**

INTRODUCTION **14**

The hippocampus 14

Place coding 15

Hippocampal-dependent and hippocampal-independent task 15

Remapping 16

Local field potential 16

SWRs and replay 17

Mechanisms of replay 18

The hippocampus in disease 19

The medial prefrontal cortex 20

Reward and goal coding 21

Planning and evaluation 22

Rule coding and rule-switching 22

Replay in the mPFC 24

Hippocampal-prefrontal interactions 24

Disconnection and inactivation studies 24

Oscillatory synchrony 25

Firing in relation to SWRs 25

Effect of mPFC lesions on hippocampal coding 26

AIM OF THE STUDY **27**

METHODS **28**

Surgery 28

Microdrive 29

Plus-maze apparatus and task 29

Behavior 31

Trajectories 31

Histology and reconstruction of recording positions 32

Data Acquisition 32

Spike sorting and unit classification 33

Linearized position 34

Theta coherence 34

Theta and gamma phase locking 34

Linearized firing rate maps 36

Cofiring similarity 36

Cofiring flickering 36

Place field similarity 37
Bayesian decoding 37
Cross-validation 38
Spiking window used for decoding 38
Confusion Matrix 38
Trajectory score 39
Shuffling procedure 40
Trajectory selection and concatenation 40
Cross-correlation 40
Trajectory replay and behavioral correlates 41
Statistics 41

RESULTS 42
Histology 42
Behavior 43
Theta and gamma oscillations 44
Theta coherence 44
Theta phase locking 45
Gamma phase locking 49
Rule remapping 52
Cofiring similarity 52
Place field similarity 55
Trajectory replay 59
Spatial coding in the HPC and mPFC 59
Replay of non-local positions 63
Replay of trajectories in the mPFC 65
Trajectory replay in the mPFC correlates with rule-switching performance 70

DISCUSSION 73
Theta and gamma oscillations 73
Rule remapping 75
Trajectory replay 78

REFERENCES 81

LIST OF FIGURES

Figure 1: Schematic representation of the excitatory pathways in the hippocampus

Figure 2: Neuroanatomical divisions of the mPFC

Figure 3: 32-tetrode microdrive for bilateral mPFC and unilateral HPC recordings

Figure 4: Rule-switching task on the plus-maze

Figure 5: Example of spike clustering performed on a HPC tetrode.

Figure 6: Histological verification of tetrode positioning in the mPFC and HPC

Figure 7: Increased errors after the rule change

Figure 8: Increased HPC-mPFC theta coherence at maze center and goal

Figure 9: Increased theta phase locking strength of HPC and mPFC cells at the maze center and goal

Figure 10: The MVL of mPFC cells does not code for rules

Figure 11: Gamma phase locking strength of HPC and mPFC pyramidal cells

Figure 12: Cofiring dynamics and rule coding in the HPC and mPFC

Figure 13: Trial-by-trial cofiring similarity to Rule 1 and Rule 2 blocks

Figure 14: Remapping dynamics and rule coding in the HPC and mPFC

Figure 15: Spatial coding in the HPC and mPFC

Figure 16: Spatial coding of the relative position in the mPFC

Figure 17: Positional decoding with HPC and mPFC spiking and its precision

Figure 18: During immobility the mPFC encoded non-local positions

Figure 19: Replay of trajectories in the mPFC during immobility

Figure 20: Alternative selection of trajectory events and their score distributions

Figure 21: Sudden change in mPFC network activity during a trajectory replay event

Figure 22: HPC and mPFC trajectory replay events do not co-occur

Figure 23: HPC and mPFC trajectory replay and rule-switching performance

Figure 24: Trajectory replay in correct and error trials

ABBREVIATIONS

AC	anterior cingulate
AP	anteroposterior
CA	cornu ammonis
DG	dentate gyrus
DISC1	Disrupted-in-schizophrenia 1
dPrl	dorsal prelimbic cortex
EC	entorhinal cortex
HPC	dorsal CA1 of hippocampus
Ifl	infralimbic cortex
LED	light-emitting diode
LFP	local field potential
ML	mediolateral
mPFC	medial prefrontal cortex
MVL	mean vector length
OFC	orbitofrontal cortex
Prl	prelimbic cortex
SEM	standard error of the mean
SD	standard deviation
SWRs	sharp wave ripples

INTRODUCTION

Navigating within an environment and learning which behavior leads to a reward, combined with the ability to flexibly adapt behavioral strategies upon changed reward contingencies, requires the interplay of brain regions. Two brain areas that are implicated in these cognitive processes are the hippocampus and medial prefrontal cortex (mPFC). Although learning and memory functions have been ascribed to most brain regions, declarative memory - the memory of facts and events - has been particularly associated with the hippocampus (Scoville and Milner, 1957; Eichenbaum, 2001). With the discovery of place cells and that hippocampal lesions cause severe impairments in spatial navigation, spatial memory, a type of declarative memory, is the most widely studied function of the hippocampus (Morris et al., 1982; O'Keefe and Dostrovsky, 1971). On the other hand, cognitive control of behavior such as attention and planning, is thought to depend on the mPFC. Flexibly switching between strategies requires cognitive control and the mPFC (Ragozzino et al., 1999a). A study demonstrating that humans with lesions to the prefrontal cortex show perseverative behavior provided early evidence for a mPFC involvement in flexibly switching between strategies (Milner, 1963).

The hippocampus and mPFC have been implicated in various behaviors, but the following introduction will focus on studies that link these areas with cognitive functions required for the performance of goal-directed behavior.

The hippocampus

The hippocampus proper is divided into the three subregions dentate gyrus (DG), CA3 (CA for cornu ammonis) and CA1. The three subregions are connected via excitatory synapses and information is routed from DG → CA3 → CA1 (Andersen, 1975). The excitatory projections connecting the DG to CA3 are called the mossy fibers and those connecting the CA3 to CA1 are the Schaffer collaterals. Most sensory information reaches the hippocampus through the entorhinal cortex (EC). The perforant path describes the input from EC layer II reaching the DG and CA3. Through the temporoammonic path input from EC layer III reaches the CA1. EC layer V is innervated by the CA1 and subiculum, making the EC also the main relay for information flow out of the hippocampus to neocortical areas.

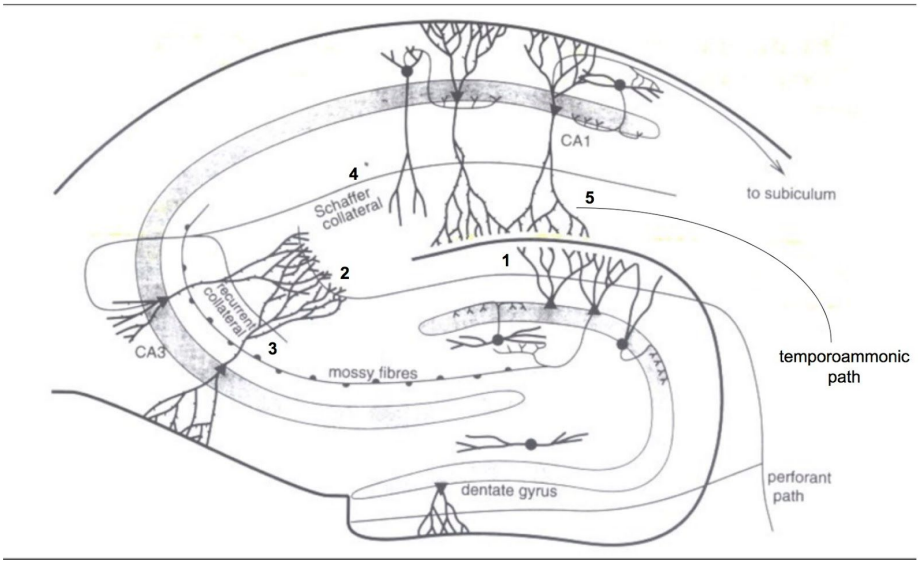

Figure 1: Schematic representation of the excitatory pathways in the hippocampus.
(**a**) Input reaches the hippocampus over the perforant path: EC layer II projects onto granule cells in the DG (1) and CA3 pyramidal neurons (2). Another input constitutes the temporoammonic path: EC layer III projects onto CA1 pyramidal neurons (5).
(**b**) Mossy fibers of granule cells project to CA3 (3).
(**c**) Schaffer collaterals of CA3 pyramidal neurons project onto CA1 pyramidal neurons (4).
(**d**) Recurrent collaterals (RC) of CA3 pyramidal neurons project to other CA3 pyramidal neurons.
(**e**) CA1 pyramidal neurons project to the subiculum and deep layers of the EC.
(Figure adapted from (Rolls and Treves, 1998).)

Place coding

A breakthrough in the field of hippocampal research came with the discovery that CA1 pyramidal cells are active in discrete places of an environment. These spatially-selective cells were named place cells and it was proposed that entire ensembles of these cells are the substrate for the cognitive spatial map required for spatial navigation (O'Keefe and Nadel, 1978; Tolman, 1948). As the number of simultaneously recorded place cells increased, it became possible to predict the spatial position of the animal based on the activity of the neural population (Wilson and McNaughton, 1993).

Hippocampal-dependent and hippocampal-independent task

Additional evidence that the hippocampus has a role in spatial processing came from lesion studies. Hippocampal lesions typically result in performance deficits for tasks with a spatial

component, whilst versions of the task without a spatial component can be solved without the hippocampus. A seminal study required rats to navigate in a pool of water positioned in a room with external landmarks and find a hidden platform for escape (Morris et al., 1982). Hippocampus lesions caused profound increases in escape latency. When the platform protruded out of the water, and thereby was made visible to the rat, the performance of hippocampus-lesioned rats reached that of controls. This Morris Water Maze study therefore demonstrated that tasks involving spatial navigation are hippocampus-dependent. Numerous subsequent studies further corroborated the notion that the hippocampus is required for spatially-guided strategies, whilst response- or cue-guided strategies are hippocampus-independent (Colombo et al., 2003; Ferbinteanu, 2016; Packard et al., 1989; Stringer et al., 2005).

Remapping

With the discovery of place cells an extensive body of studies investigated their properties further. In particular, the stability of place cell coding was first tested by comparing their spatial firing fields, i.e., place fields, at various exposures to the same environment. Indeed, place cells would show stable firing patterns over days if the environment was kept constant (Muller et al., 1987). However, changes to visual cues and the environment lead to the appearance, disappearance or moving of place fields, a phenomenon termed global remapping (Muller and Kubie, 1987). Later it was found that place cells also showed variations in firing rates, without changing their spatial selectivity, which was termed rate remapping. Remapping does not only result from changes in sensory cues but also motivational state and behavioral context (Markus et al., 1995; Wood et al., 2000). Therefore, the hippocampus can separate memories by providing distinct representations for similar environments via remapping. Global and rate remapping will lead to changes in the temporal firing relationship between cells. Co-firing between cell pairs is therefore also measured when investigating for changes in population coding (Averbeck et al., 2006).

Local field potential

The electrophysiological signal arising from the summed electrical activity of many nearby neurons is called the local field potential (LFP). The LFP can oscillate at different frequencies that are associated with cognitive functions. Theta oscillations (6-10 Hz) represent a prominent pattern of hippocampal activity that, in rodents, mainly arise during

voluntary movement such as running (Vanderwolf, 1969). The theta phase at which hippocampal cells fire provides additional information (Huxter et al., 2008; Lever et al., 2010; O'Keefe and Recce, 1993). Another prominent pattern in the hippocampal LFP, specifically in CA1, are the sharp wave-ripples (SWRs), which are transient (50-100 ms) and fast (150-250 Hz) oscillatory events (Buzsaki et al., 1992). During SWRs pyramidal and interneurons exhibit burst firing, leading to periods of high synchrony among the hippocampal population (Buzsaki et al., 1992). SWRs primarily occur during slow-wave sleep and behavioral immobility, such as exploratory pauses or consummatory behavior (Buzsaki et al., 1992; Csicsvari et al., 1999). Tonic excitation from CA3 and phasic inhibition within CA1 underlie the generation of CA1 SWRs (Gan et al., 2017).

SWRs and replay

The finding that hippocampal neurons exhibit burst firing during SWRs, led to the question of whether cells randomly participated in increased firing or whether a selective group of cells was active during these events. First indication that firing during sleep may serve a mnemonic function came from a study showing that hippocampal cells that were active during the waking period would increase their firing rate in subsequent sleep (Pavlides and Winson, 1989). Later it was shown that place cell pairs that had overlapping place fields, and hence fired together with short latencies during waking, also showed an increased tendency to fire together in subsequent sleep, representing a cellular correlate of learning (Wilson and McNaughton, 1994; O'Neill et al., 2008). The reactivation of awake cell pair co-firing in sleep was larger during SWRs than compared to the rest of sleep. Finally, it was demonstrated that the order of reactivation is maintained in sleep SWRs and can replay entire spatial trajectories in a time-compressed manner (Louie and Wilson, 2001; Skaggs and McNaughton, 1996). The role of sleep replay is thought to lie in the consolidation of memories for behavioral events. Indeed, reactivation of goal-related hippocampal assemblies in sleep predicts later goal memory and selective disruption of SWRs during sleep impairs spatial learning and memory (Dupret et al., 2010; Ego-Stengel and Wilson, 2010; Girardeau et al., 2009).

Replay was later also demonstrated to occur during periods of immobility during the awake state. The firing rate of hippocampal cells was increased during awake SWRs as was the cofiring of cell pairs with neighboring place fields (O'Neill et al., 2006). Finally, hippocampal replay of entire trajectories could also occur during awake SWRs (Diba and Buzsáki, 2007; Foster and Wilson, 2006; Pfeiffer and Foster, 2013; Singer et al., 2013). Several functional

roles have been proposed for awake replay in the hippocampus. For example, reactivation during awake SWRs was enhanced after rewarded outcomes, suggesting that awake replay might have a role in assigning value to places (Ambrose et al., 2016; Singer and Frank, 2009). Awake replay might facilitate storage of new memories since novel experiences also enhance reactivation (Cheng and Frank, 2008). Finally, there is increasing evidence that awake replay supports planning of future paths and goal-directed behavior. Awake replay was increased at the decision point before correct choices and inhibition of awake SWRs resulted in impairments in the learning of a spatial alternation task (Jadhav et al., 2012; Singer et al., 2013). Interestingly, reactivated trajectories at the decision point included both the upcoming correct arm as well as the other not chosen arm and were therefore not predictive of the behavioral choice (Singer et al., 2013). Later studies however did demonstrate that awake replay can be predictive of choice (Pfeiffer and Foster, 2013; Xu et al., 2019). The Xu et al. study, for instance, found that replay at the choice point in the reference memory version of the radial maze was predictive of the future arm taken, whilst in the working memory version of the task was predictive of the past arm (Xu et al., 2019). Further evidence that awake replay is not a mere recapitulation of experience, but may have a role in planning or evaluating choices, came from studies that showed that replay was not necessarily linked to ongoing behavior and could replay previously not-experienced trajectories and even trajectories avoided by the animal (Gupta et al., 2010; Pfeiffer and Foster, 2013; Wu et al., 2017).

Mechanisms of replay

The mechanisms that underlie replay remain controversial. Whilst one line of evidence suggests that replay is generated from experience (Silva et al., 2015), others suggest that replay reflects preconfigured and hardwired assemblies (Dragoi and Tonegawa, 2011). The study of Dragoi and Tonegawa coined the term preplay, where place cell sequences in a novel environment can already be found in sleep preceding novel environment exploration (Dragoi and Tonegawa, 2011). According to this finding, place sequences during behavior reflect a pre-configured temporal order of place cells, diminishing the role of experience in replay and thus a role of replay in learning and memory. A follow-up study by Silva et al. performing large-scale hippocampal recordings, however demonstrated that experience is required for trajectory events in the hippocampus. They report that post-experience, and not pre-experience, replay events were better correlated with behavior and that post-experience events were less jumpy and more linear. Since larger numbers of recorded cells allow the

detection of smoother trajectories, a low number of cells in the preplay studies might have prevented the observation that post-experience events contained better trajectory replay than pre-experience events. Finally, these two competing views could be reconciled with the finding that place cell sequences during novel environment exploration contained firing of both, cells that contributed to sequence replay before and thus are hard-wired, and plastic cells that are added (Grosmark and Buzsáki, 2016). Similarly, post-task sleep replay consisted of rigid cells that were present during pre-task sleep and the task, and the plastic cells that were added to the preexisting backbone, thus adding an experience dependency to replay (Grosmark and Buzsáki, 2016).

Since replay is the reactivation of behavioral experiences it (so far) could not be studied in vitro and thus its synaptic mechanisms are poorly understood. However, considering that experience determines the content of replay, it suggests that during behavior certain synaptic modifications between place cells occur that lead to their subsequent reactivation. NMDA-receptors are required for activity-dependent synaptic modifications and when activated can lead to strengthening or weakening of synapses (Banerjee et al., 2016; Lüscher and Malenka, 2012). Indeed, blocking of NMDA receptors during goal-learning prevented subsequent enhanced replay of goal locations resulting in memory deficits (Dupret et al., 2010) and NMDA-receptor blocking during exploration abolished sequential replay without impairing the spatial coding of place cells (Silva et al., 2015). Additionally, replayed sequences are temporally compressed, providing the temporal window for spike-timing-dependent plasticity mediated by NMDA-receptors. Together, NMDA receptor-dependent strengthening of synapses between cells during behavior may thus facilitate their later reactivation. However, since the hippocampus can replay trajectories that have never been experienced, replay is not just the reactivation of cells with synapses strengthened by experience (Gupta et al., 2010; Pfeiffer and Foster, 2013). It may rather represent the attempt to access information from a learned cognitive map (Silva et al., 2015).

The hippocampus in disease

When studying the effects of a disease on brain function, studies often investigate how the above-mentioned computations of the hippocampus are altered in the disease state. First an animal model of the studied disease is generated and then electrophysiological recordings performed. An example of such a study investigated how aggregation of the Disrupted-in-schizophrenia 1 (DISC1) protein in the brain, a model of chronic mental illness,

alters hippocampal function (Kaefer et al., 2019). Rats transgenically overexpressed the DISC1 gene (tgDISC1 rats), which led to DISC1 protein aggregations in brain areas including the hippocampus and disturbances in the dopaminergic system. The activities of pyramidal cells were recorded from the dorsal CA1 of the hippocampus whilst tgDISC1 rats explored a familiar and novel environment and during sleep. The study found that the size of place cell firing fields was smaller in tgDISC1 rats, improving their place coding precision. However, tgDISC1 place cells were impaired in coding for location-independent information such as the running speed of the animal. Furthermore, tgDISC1 cells did not exhibit a shift in preferred theta oscillation firing phase, which is observed in control animals upon novel environment exploration. Finally, during sleep SWRs, pyramidal cells of tgDISC1 rats had a lower firing rate than those of controls. This study demonstrates that increasing knowledge about hippocampal functioning also advances our understanding of the mechanisms underlying brain-related diseases.

The medial prefrontal cortex

Although the neocortex of the rat can have six layers, the prefrontal cortex does not exhibit the granular layer four. It was therefore long debated whether rats have a prefrontal cortex, because layer four was regarded as the major input area of thalamic projections and hence the beginning of information processing in the cortex. However, the rat prefrontal cortex qualifies as such because other layers form connections with the thalamic mediodorsal nucleus (Uylings et al., 2003). The prefrontal cortex is divided into three agranular regions, the orbital, insular and medial part of the frontal cerebral hemispheres. The medial prefrontal cortex (mPFC) further divides from dorsal to ventral into the anterior cingulate (AC), prelimbic area (Prl), infralimbic area (Ifl) and medial orbitofrontal cortex (OFC). The Prl and Ifl together, as opposed to the AC and OFC, are the mPFC regions that have been most associated with switching and coding of rules (see ‘Rule coding and rule-switching’ section). Additionally, neural population changes related to rule-switching were reported to first occur in the Prl and only then in the Ifl (Rich and Shapiro, 2009). Therefore, in this study, recordings were specifically performed in the Prl of the mPFC. In the following, when reporting results from other studies on mPFC, brackets indicate which mPFC division their work refers to.

Retrograde tracing studies showed that the input the mPFC receives differs along it dorsoventral axis (Hoover and Vertes, 2007). The AC receives increased sensorimotor input

from widespread cortical areas and their associated thalamic nuclei. The Prl and Ifl receive less sensorimotor, but increased input from the perirhinal and entorhinal cortices, the hippocampus, basal nuclei of the amygdala, the thalamus (to layer three, five and six) and brainstem monoaminergic nuclei (Heidbreder and Groenewegen, 2003; Hoover and Vertes, 2007).

Pyramidal cells of layer two and three of the prefrontal cortex project to other cortical areas. Subcortical areas are targeted by layer five pyramidal cells, whilst the thalamus receives its prefrontal input mainly from layer six (but also layer three). Anterograde tracing studies demonstrated that the Prl and Ifl share only a few common output areas. The Prl and Ifl both project to the OFC and midline thalamus. Some of the main projection sites of the Prl are the nucleus accumbens, mediodorsal thalamus, nucleus reuniens, the amygdala, and the dorsal and median raphe nuclei of the brainstem (Vertes, 2004).

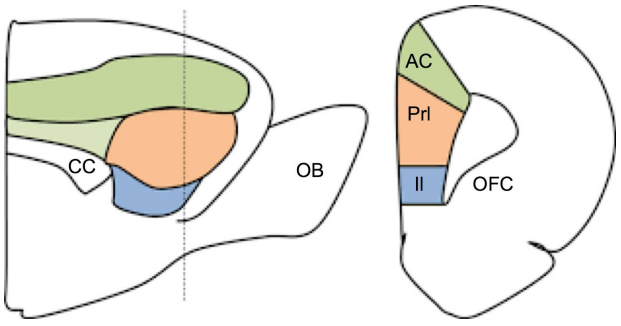

Figure 2: Neuroanatomical divisions of the mPFC.
Sagittal (left) and coronal (right) sections of the mPFC showing the anterior cingulate (AC), prelimbic (Prl), infralimbic (Il) and orbitofrontal (OFC) cortices. The dotted line on the sagittal view denotes the location of the coronal section. CC, corpus callosum; OB, olfactory bulb. Scheme adapted from (McKlveen et al., 2015).

Reward and goal coding

Learning and performance of goal-directed behaviors requires encoding of goals and recognition of which behaviors lead to the desired outcome and which do not. Studies have found that the mPFC codes for reward, approach and departure from reward areas and relative value of reward (Jung et al., 1998; Pratt and Mizumori, 2001). One study demonstrated that the mPFC does not just code for reward consumption but actual spatial goals. Their task required rats to enter an unmarked zone in an open field to trigger an

overhead feeder to release a food pellet, which could fall anywhere on the maze (Hok et al., 2005). They found that cells of the mPFC (Prl + Ifl) had discrete place fields mostly around the goal zone, demonstrating that mPFC cells have goal selectivity that is not directly related to reward consumption. This study also showed that the mPFC has spatial selectivity.

Planning and evaluation

Unexpected outcomes, such as a large rewards or no reward at all, are encoded in mPFC neurons of monkeys primarily with increases in firing rates (Asaad and Eskandar, 2011). In rats the firing rates of mPFC cells are also modulated by errors and a decrease in anticipatory firing at reward absences has been reported, indicating some sort of outcome evaluation (Narayanan and Laubach, 2008; Pratt and Mizumori, 2001; Sul et al., 2010). Population vector analysis showed that as learning in a continuous T-maze improved so did decoding of the past and future goal from central stem activity (Baeg et al., 2003). However, correlating neural ensembles occurring in the central stem of correct and error trials, showed that they were only significantly different when the past and not future goal was different. These findings therefore support a prefrontal role in past choice evaluation rather than in planning and indicate that future goal decoding was only possible due to the high stereotypy of the task. Similarly, prediction of a future goal from mPFC neurons (AC, Prl, Ifl, OFC) was weak on the central arm of a T-maze and increased steeply once the trajectories diverged (Sul et al., 2010). However, others did find trajectory-dependent firing in the mPFC (AC, Prl) that was not explained by variances in running behavior, such as lateral position, and hence provide evidence for a planning role of the mPFC (Ito et al., 2015). The same study lesioned the nucleus reuniens, a thalamic area that connects the Prl and dorsal hippocampus and that also shows trajectory-dependent firing. Nucleus reuniens lesioning lead to the disruption of trajectory-dependent firing in the dorsal CA1, suggesting that representations of future paths are passed on from the mPFC to the dorsal CA1.

Rule coding and rule-switching

Early indications that the mPFC is involved in flexible learning came from patients with dorsolateral frontal lobe damage performing the Wisconsin Card Sorting Task. In this test subjects are given a set of cards displaying different shapes that also vary in color and number. The subjects are not told according to which of these dimensions the cards should be sorted, but through the experimenter's feedback quickly learn. The sorting rule is then

changed without informing the subject, who then typically realizes the rule change and flexibly shifts to a different sorting strategy. Patients with dorsolateral frontal lobe damage performed poorly compared to controls (Milner, 1963). Similarly, studies that lesioned or inactivated the mPFC in rats found that this brain area was critical for flexible rule-switching in various behavioral tasks (Birrell and Brown, 2000; de Bruin et al., 1994; Ragozzino et al., 1999a, 1999b). Interestingly, these studies showed that the mPFC was not required for the initial learning of the task and that it was specifically required for extra-dimensional rather than intra-dimensional rule-switching (i.e., from spatial to cue-guided and not spatial-east to spatial-west) (but see (Guise and Shapiro, 2017) which found deficits in intra-dimensional switch).

Further evidence for a mPFC involvement in rule-switching came from electrophysiological studies. Neural correlates for rule coding have been reported for mPFC (Prl, Ifl) cells that distinguished between two rules with their firing (Bissonette and Roesch, 2015; Durstewitz et al., 2010; Rich and Shapiro, 2009). Increased firing rate during high conflict trials was also reported for mPFC cells (Bissonette and Roesch, 2015).

Beyond single neuron correlates, studies recording from a large population of neurons reported changes in the mPFC network state following rule switches. The first study to report Prl neural population changes during rule-switching was on rats that had to shift from a light-guided to an egocentric strategy in a lever task. With firing rate population vectors, the study found that neural ensembles distinguished between the two rules (Durstewitz et al., 2010). Furthermore, often during learning of the new rule the Prl population showed an abrupt rather than gradual transition to the neural representation of the novel rule, indicating moments of sudden insight. One explanation for this finding is that an accumulation of errors may lead to a destabilization of one Prl network state and the emergence of another corresponding to the new rule. Another study found that when rats abandoned an old rule and started exploring new strategies, neurons of the AC would coordinately show transient changes in their firing rate (Karlsson et al., 2012). These unexpectedly large firing rate changes spanned several trials and accompanied periods with increased errors when new strategies were tested. The network transitions may therefore reflect behavioral uncertainty or newly established beliefs, and confidence and hence good performance may come gradually due to the probabilistic nature of their task. Support for this comes from a study showing that rule switch-related changes in mPFC (Prl) representation occurred before a change in the animal's behavior, indicating that mPFC may code for the need of changing a

strategy rather than the actual strategy shift itself (Powell and Redish, 2016). However, a study comparing mPFC (Prl) activity in sleep before and after performance on a Y-maze showed that population activity always changed irrespective of whether the animal experienced a rule switch or not (Singh et al., 2019).

Replay in the mPFC

Replay has also been shown for the mPFC population. This was first demonstrated in sleep where previous behaviorally-driven firing sequences of neuronal assemblies become reactivated in subsequent rest periods (Euston et al., 2007). All other studies investigated mPFC replay in conjunction with SWRs and associated hippocampal replay and will therefore be discussed below in the hippocampal-prefrontal interactions section.

Hippocampal-prefrontal interactions

Interactions between the Prl and hippocampus can occur through direct or indirect connections. Injecting retrograde tracers into the Prl showed that this area receives prominent direct projections from the ventral CA1 and proximal subiculum (Hoover and Vertes, 2007). The Prl does not directly project back to the hippocampus. It instead connects to the dorsal and ventral CA1 indirectly and bidirectionally via the thalamic nucleus reuniens (Varela et al., 2014; Vertes et al., 2006; Xu and Südhof, 2013) and via the perirhinal and lateral entorhinal cortices (Delatour and Witter, 2002; Hoover and Vertes, 2007). Recently, sparse direct connections from the dorsal CA1 to Prl have also been reported (Ye et al., 2017). Connectivity studies therefore provide indications for a bidirectional flow of information between the Prl and the dorsal CA1.

Disconnection and inactivation studies

Direct evidence that the hippocampus and mPFC functionally interact comes from crossed lesion studies. With crossed lesions each area is lesioned or inactivated in opposite hemispheres, leaving one of the two areas intact in one hemisphere, but preventing ipsilateral communication between them. Inactivating ipsilateral hippocampal-mPFC communication lead to performance deficits in the delayed-version of the radial maze that were not present when only one of the two areas was inactivated unilateraly (Floresco et al.,

1997). Selectively inactivating the ipsilateral connection between the dorsal hippocampus and mPFC resulted in temporal order memory deficits, whilst inactivating the ventral hippocampus to mPFC ipsilateral connection caused deficits in spatial memory (Barker et al., 2017). Finally, optogenetic inactivation of ventral CA1 projections to the mPFC (Prl + Ifl) resulted in specific deficits in spatial encoding during a T-maze task (Spellman et al., 2015).

Oscillatory synchrony

Early electrophysiological evidence for a functional interaction between the mPFC and hippocampus came from a study that simultaneously recorded hippocampal LFP and mPFC cell spiking activity whilst the animal performed a variety of spatial tasks. This study reported that mPFC cells preferentially fired at certain phases of hippocampal theta oscillations and hence were phase locked (Siapas et al., 2005). In a spatial working-memory task it was then shown that hippocampal theta phase locking of mPFC cells and hippocampal-mPFC theta coherence was highest on correct trials, and lower on error trials and during the working memory-independent version of the task (Jones and Wilson, 2005). Further evidence for a role of mPFC and hippocampus theta synchronization in memory-guided processes came from a study involving a rule-switching task that reported increased hippocampal-mPFC theta synchronization and coincident mPFC (Prl) cell pair coactivation after acquisition of a new rule (Benchenane et al., 2010). Furthermore, only upon successful rule learning did mPFC (Prl) cells change their firing relative to hippocampal theta oscillations (Benchenane et al., 2010). Finally, the directionality of hippocampal-mPFC information flow differs with different cognitive demands. Theta amplitude cross-correlation analysis indicated that information goes from the hippocampus to mPFC during contextual retrieval and from the mPFC to hippocampus during retrieval of context-appropriate hippocampal memory (Place et al., 2016).

Firing in relation to SWRs

Evidence for a functional relationship between hippocampal SWRs and mPFC firing came from a study employing a rule-switching task that found that mPFC (Prl) firing patterns present after acquisition of a new rule were preferentially replayed in subsequent sleep during hippocampal SWRs (Peyrache et al., 2009). During sleep, mPFC firing was also increased 100 ms after hippocampal SWRs indicating a possible role in memory consolidation (Wierzynski et al., 2009). Firing of mPFC neurons are also modulated by

awake SWRs. mPFC (Prl) pyramidal cells can exhibit excitation or inhibition upon awake SWR occurrence, and hippocampus-mPFC cell pairs that are spatially correlated are also more correlated during awake SWRs (Jadhav et al., 2016). The functional role of interactions between the mPFC and SWRs is likely different for the awake and sleep state. The coordination of hippocampus and mPFC (Prl) cells was stronger for awake than sleep SWRs, indicating that coordination during awake SWRs may serve accurate memory storage and memory-guided behavior, whilst coordination during sleep SWRs may rather support integration of memories across different experiences (Tang et al., 2017). Finally, mPFC cells coding for generalized task features were more likely to participate in hippocampal replay (Yu et al., 2018).

Effect of mPFC lesions on hippocampal coding

Lesion and inactivation studies provide final evidence that neural computations in the hippocampus and mPFC depend on each other. Recordings from the hippocampus of rats with mPFC (AC + dPrl) lesions showed that place fields were less stable over time, demonstrating that the mPFC is involved in hippocampal spatial firing responses (Kyd and Bilkey, 2003). Another study inactivated the mPFC (Prl + Ifl) with lidocaine and found that place cell firing variability was decreased (Hok et al., 2013). Non-spatial information, such as episodic memory, is reflected in the firing variability of place cells, therefore the mPFC might also be involved in location-independent coding of the hippocampus (Leutgeb et al., 2005). Finally, two studies indicate that hippocampal selectivity is modulated by the mPFC. In a task in which spatial context guides a rat which of two food wells contains reward, dorsal CA1 cell firing reflects specific object-location associations. Object selectivity of hippocampal cells decreased with mPFC (Prl) inactivation, resulting in cells that in a given context previously fired around one specific object, fire at both objects (Navawongse and Eichenbaum, 2013). Interestingly, the spatial location of firing in relation to the object did not change with mPFC (Prl) inactivation. In the other study, rats were trained to collect reward on a plus-maze based on two spatially-guided strategies. The activity of the hippocampus in the start arm distinguished between the two prospective goals, but upon mPFC (Prl) inactivation dorsal CA1 trajectory-dependent firing weakened (Guise and Shapiro, 2017). Trajectory-dependent information is thought to reach the dorsal CA1 from the Prl via the nucleus reuniens (Ito et al., 2015). A study showing that inhibition of ventral CA1 projections to the mPFC (Prl + Ifl) caused deficits in spatial encoding demonstrates that the mPFC also receives task-related information from the hippocampus (Spellman et al., 2015).

AIM OF THE STUDY

Navigating within an environment and learning which behavioral response leads to a reward, combined with the ability to flexibly change behavioral strategies upon changed reward contingencies, require the involvement and interaction of more than one brain area. The hippocampus has extensively been shown to have a role in learning and memory, particularly for spatial information. The ability to flexibly switch between behavioral strategies, on the other hand, has been ascribed to the mPFC. The plus-maze rule-switching task was designed to elicit cognitive processes subserved by both the hippocampus and mPFC. In this task a rat had to navigate towards one of two goals, depending on whether a spatial or light-guided rule was employed. Following an unannounced change in rule, the rat had to abandon the old strategy, find out according to which rule the reward is hidden and switch to the new strategy. We recorded local field potentials and single unit activity simultaneously from the dorsal hippocampus CA1 (HPC) and the Prl of the mPFC, whilst rats performed the plus-maze task. By recording the neural activity of the HPC and mPFC in a task that engages these two areas, the neural computations underlying solving of this task can be investigated. Furthermore, by comparing the activities in these two areas their specialized roles for the successful performance of this task can be delineated.

We focused on three prominent activity patterns that have been described for the hippocampus: oscillations (theta and gamma), remapping and trajectory replay. The analyses performed are divided into the following three chapters with their specific aims:

1. Characterize theta and gamma oscillatory interactions between the HPC and mPFC during the hippocampus-dependent and hippocampus-independent version of the task.
2. Quantify remapping dynamics in the HPC and mPFC during rule-switching.
3. Investigate replay of trajectories in the HPC and mPFC during rule-switching.

METHODS

Surgery

All procedures involving experimental animals were carried out in accordance with Austrian animal law (Austrian federal Law for experiments with live animals) under a project license approved by the Austrian Federal Science Ministry (License number: BMWFW-66.018/0015-WF/V3b/2014).

Four male Long-Evans rats (300-350 g) were implanted with microdrives housing 32 individually-movable tetrodes. The tetrodes were arranged into three bundles targeting the right dorsal hippocampus (specifically dorsal CA1, in the analysis referred to as “HPC”) and left and right mPFC (specifically Prl, in the analysis referred to as “mPFC”). Each tetrode was fabricated out of four 12 um tungsten wires (California Fine Wire Company, Grover Beach, CA) that were twisted and then heated to bind into a single bundle. Tetrode bundle lengths were cut so that the two mPFC bundles were 1-1.5 mm longer than the hippocampus bundle. The tips of the tetrodes were gold-plated to reduce the impedance to around 300 kΩ. Before commence of surgery the animal was put under deep anesthesia using isoflurane (0.5–3%), oxygen (1–2 L/min), and an initial injection of buprenorphine (0.1 mg/kg body weight) and ketamine/xylazine (7:3 ketamine (10%) and xylazine (2%), 0.05 ml/100 g). Craniotomies were drilled above the hippocampus (anteroposterior (AP): -2.50 to -4.50, mediolateral (ML): -1.2 to -3.6) and above the mPFC across the sinus (AP: 4.60 to 2.50, ML: 0 to ± 0.8). Six anchoring screws were fixed onto the skull and two ground screws were positioned above the cerebellum. After dura removal the tetrode bundles were centered above their respective craniotomies and lowered into the brain at a depth of ~2 mm for the mPFC and ~1 mm for the hippocampus. The exact depth of mPFC tetrode implantation was noted to ensure later lowering into the target area. Tetrodes and craniotomies were coated in paraffin wax and the microdrive was anchored to the skull and screws with dental cement. The analgesic meloxicam (5 mg/kg body weight) was given up to three days after surgery and the animal was allowed one week recovery. Thereafter, tetrodes were gradually moved in 50-200 µm steps into the hippocampal CA1 pyramidal cell layer and Prl of the mPFC.

Microdrive

To increase the yield of recorded cells we used 32-, instead of the standard 16-tetrode drives. The mPFC shuttles were arranged in a way that the eight tetrodes of each bundle are confined to the area of the Prl. Furthermore, the distance between the two bundles was 0.8 mm, approximately the width of the sinus. Ensuring that each mPFC tetrode bundle was positioned adjacent to the sinus allowed recordings of cells also from the outer layers. The hippocampus bundle was arranged so that it was confined to the dorsal hippocampus. The microdrive was designed and manufactured by Todor Asenov and Thomas Menner of the IST Austria Miba Machine shop.

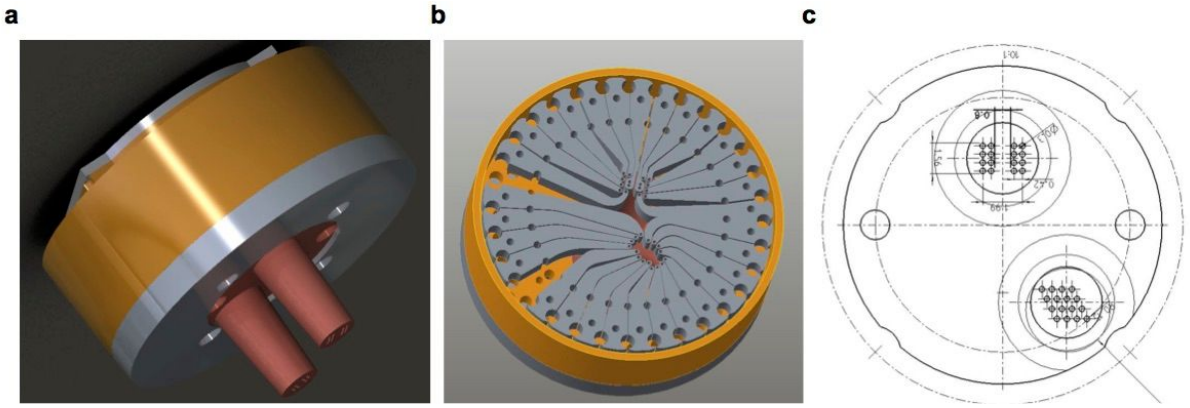

Figure 3: 32-tetrode microdrive for bilateral mPFC and unilateral HPC recordings.
(**a**) Outside view of microdrive, where one cylinder targets the HPC and the other the mPFC.
(**b**) Top view of the shuttles. The upper 16 shuttles target the left and right hemisphere mPFC and the lower 16 shuttles target the right hemisphere HPC.
(**c**) Bottom view of cannulae exit holes. Top and bottom shows the exit holes for the mPFC and HPC respectively.

Plus-maze apparatus and task

Animals were housed individually in a separate room under a 12h light/ 12h dark cycle. Following the recovery period, animals were food-restricted to 85% of their pre-surgery weight, with ad libitum access to water and accustomed to the plus-maze and rest box. The plus-maze was elevated (80 cm) and consisted of four arms (83 cm long and 12 cm wide) referred to as north, east, south and west and a connecting center. Visual cues were mounted on the walls of the experimental room for spatial orientation. The animal was placed in one of the two start arms (north or south) and had to collect food reward (MLab rodent tablet 20 mg, TestDiet, Richmod, USA) in one of the two goal arms (east or west),

depending on the rule employed (**Figure 4b**). Access to the arm not chosen as the start was restricted, so that the maze became T-shaped. The distance from start to goal arm was 200 cm. A small light at the end of one of the two goal arms was switched on. Which arm was chosen as the start and light-on arm was chosen pseudorandomly for every trial, ensuring that an arm was not chosen more than three consecutive times. Once the animal reached a goal arm and ~5 s passed, it was manually returned to the rest box before commence of the next trial. The animal had to retrieve the reward based on a spatial or response (light) rule. During the spatial rule the reward was always placed in either the east or west arm, whilst during the light rule the reward was placed in the light-on arm. Importantly, also during the spatial rule one of the two arms was lit, but did not necessarily indicate the location of reward. To prevent an odor-guided strategy pellet dust was scattered along the maze and pellet-filled cups invisible to the animal placed under both goal arms. On each recording day the animal underwent behavioral blocks as follows: rest, rule 1 (remote recall), rest, rule-switch, rest, rule 2 (recent recall), rest. The rule-switch block was further divided into pre-switch, switching and post-switch (**Figure 4a).** Rest periods were 40 mins in duration, except for the last rest period of every recording day, which was 20 mins. During rule 1 (remote recall) the last rule of the previous day applied. Then during the rule-switching block, the animal had to first collect reward based on rule 1 (pre-switch) before the rule switched and reward had to be collected based on rule 2 (switching, post-switch). Begin of good performance marked the beginning of the post-switch block (see Methods - Behavior). The switch in rule was not announced to the animal, which had to learn the new rule by trial-and-error. Finally, during rule 2 (recent recall), the newly learnt rule applied. The animal had to perform cross-modal switches, i.e., switches from spatial to light or light to spatial rule, never between the two spatial rules. Reaching of the performance criterion marked the end of a rule block (counting trials of the switching and post-switch block together, and except for the recent recall (rule 2) block). Note, that whilst correct performance of a spatial rule involves two trajectories (e.g., go-east rule: north-to-east and south-to-east), correct performance of the light rule can involve any of the four trajectories. Therefore, performance criterion for the spatial rule was set to 12/15 and for the light rule to 24/30 correct trials, ensuring similar number of light rule trials where the animal performed trajectories that matched those of the spatial rule (see Methods - Trajectories). In the rule 2 (recent recall) block the number of trials was fixed to 20, providing a setting in which the animal experienced the same number of trials, irrespective of rule type.

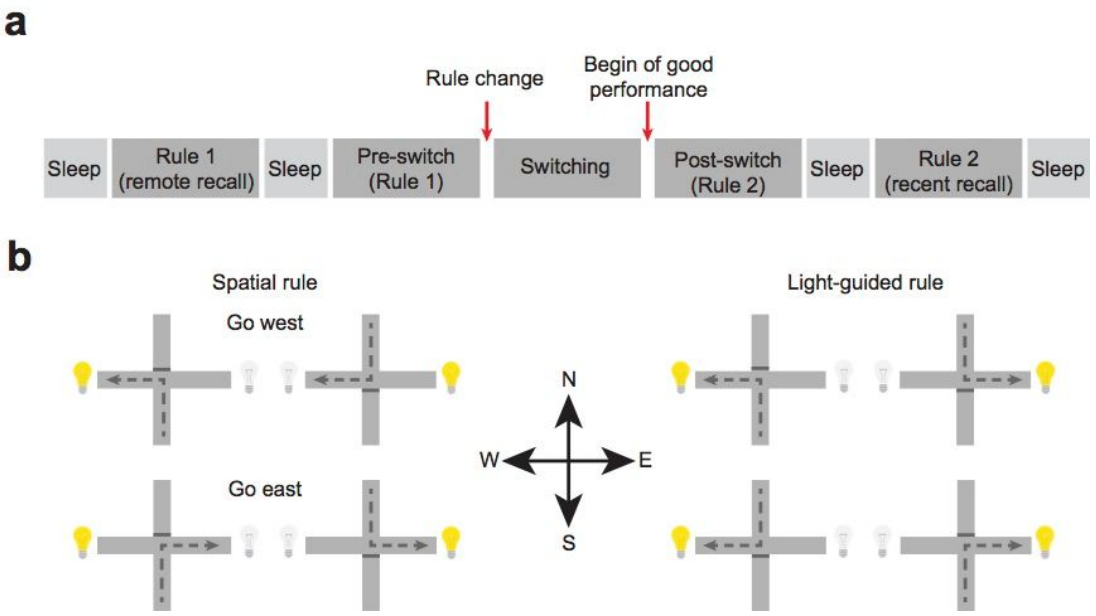

Figure 4: Rule-switching task on the plus-maze.

(**a**) Daily behavioral protocol.
(**b**) Plus-maze task. The animal had to run down one of the two start arms (south or north), approach the maze center and choose one of the two goal arms (east or west). Reward had to be collected based on a spatial (go west, go east) or light-guided strategy. Also during the spatial rule one goal arm light was switched on, but had to be ignored by the animal.

Behavior

The rule-switching block consisted of a pre-switch, switching and post-switch block (**Figure 4a**). All trials before the rule switch comprised the pre-switch block. Trials performed after the switch to the new rule, but before the animal reached good performance comprised the switching block. The beginning of good performance (bgp) was defined as the center index after rule change where the error rate over five consecutive trials dropped to zero.

$$bgp = argmin_{t \in \{trials > switch\}} \left\{ \sum_{k=-2}^{2} error(t+k) == 0 \right\} \quad (1)$$

Trajectories

Correctly performed trials of the spatial rule will include two possible trajectories. For example, if the go-east rule applied, then only trajectories from north-to-east and south-to-east will lead to a correct trial. Conversely, since the light-on arm can be in the east or west, correctly performed trials in the light rule will include all four possible trajectories

(north-to-east, north-to-west, south-to-east, south-to-west). When comparing neural activity between different rules one has to ensure that any differences observed are not due to different behaviors resulting from different trajectories. Therefore only those light-rule trials were considered for analysis that matched the trajectories from correct trials of the spatial rule. For example, if the spatial rule in a recording session was the go-east rule, then only those correct light rule trials were selected where the light-on arm was in the east and hence had trajectories either from north-to-east or south-to-east. This selection of light rule trajectories was done for parts of the phase locking (**Figure 10**) and rule remapping analysis (**Figure 12-14**).

Histology and reconstruction of recording positions

After the last recording day tetrodes were not moved. Animals were administered ketamine/xylazine (7:3 ketamine (10%) and xylazine (2%), 0.1 ml/100 g body weight), overdosed with pentobarbital and then transcardially perfused with 0.9% saline followed by 4% formaldehyde. Brains were extracted and stored in 4% formaldehyde. On the same day brains were transferred into 30% sucrose solution until sinking for cryoprotection. Finally, shock-frozen brains were cut into coronal sections with a cryostat (50-60 µm), mounted on glass slides and stained with cresyl violet. The positions of tetrode tips were determined from stained sections and cells recorded from tetrodes outside the Prl areas of the mPFC were excluded from analysis. For cells recorded from HPC tetrodes the presence of SWRs in the field recordings served as the inclusion criteria.

Data Acquisition

Extracellular electric signals from the tetrodes were pre-amplified using a headstage (4 × 32 channels, Axona Ltd, St. Albans, Hertfordshire, UK). Wide-band (0.4 Hz–5 kHz) recordings were taken and the amplified LFP and multiple-unit activity were continuously digitized at 24 kHz using a 128-channel data acquisition system (Axona Ltd). Two red LED bundles mounted on each side of the preamplifier head-stage were used to track the location of the animal. Every day before recording, tetrodes were moved optimizing the yield of recorded cells. Additionally, mPFC were lowered every day by ~30-50 µm to ensure recording of a new population of cells.

Spike sorting and unit classification

Clustering of neuronal spikes and unit isolation procedures were described previously (Csicsvari et al., 1998). Briefly, the raw data was resampled to 20 kHz and the power in the 800-9000 Hz range was computed for sliding windows (12.8 ms). Action potentials with a power of > 4 SD from the baseline mean were selected and with principal component analysis their spike features extracted. Based on their spike features, action potentials were then clustered into multiple putative units using an automatic clustering software (http://klustakwik.sourceforge.net (Harris et al., 2000)). The generated clusters were then manually refined using a graphical cluster-cutting program and only units with clear refractory periods in their autocorrelation, well-defined cluster boundaries and stability over time were used for further analysis (**Figure 5**). An isolation distance (based on Mahalanobis distance) was calculated to ensure that spike clusters did not overlap (Harris et al., 2000). Putative excitatory pyramidal cells and putative inhibitory interneurons were discriminated using their auto-correlograms, firing rates and waveforms. In the present analysis 1025 HPC and 817 mPFC pyramidal cells (of which 368 right and 449 left hemisphere mPFC) were included. No analysis was performed on putative inhibitory neurons.

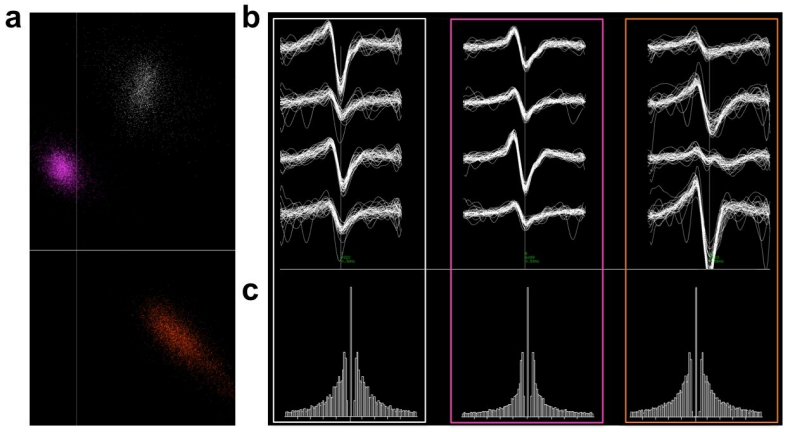

Figure 5: Example of spike clustering performed on a HPC tetrode.

(**a**) Separation of spikes into three well-defined clusters using principal component analysis. The three clusters are colour-labelled (white, magenta and orange).

(**b**) Waveforms of the three clusters recorded from the four channels of a tetrode. A broad waveform and non-linear repolarization are indicative of putative pyramidal cells.

(**c**) Auto-correlograms of the same three clusters showing burst firing typical of HPC pyramidal cells.

Linearized position

To linearize the behavior of the animal, we calculated the distance from the center from the 2D spatial position of the animal. This way a “V-shaped” positive function for each trial was obtained. For each position before the center (i.e., before the global minimum) we subtracted the minimum and then changed the sign. Then, 100 was added to every position to obtain a positive measure of the relative position of the animal between start (0 cm) and goal (200 cm). The center corresponded to 100 cm.

Theta coherence

LFP data from one channel of each tetrode was divided into 2000 ms time windows with an overlap of 1600 ms. The spectral coherence between all possible HPC and mPFC channel pairs was computed for each window of a trial using the multitaper function from Matlab’s chronux toolbox (Matlab version 2017, http://chronux.org). Coherence values for each time window of a trial were allocated to their respective 5 cm spatial bin of the linearized maze and an average coherence for each frequency between 1 and 475 Hz was computed for each spatial bin of a trial. The theta frequency coherence (6-10 Hz) was extracted for each spatial bin of a trial. Error trials were excluded. Separately for every session, the mean theta coherence over all the trials was calculated for every spatial bin. Finally, a theta coherence mean and SEM was computed over all the session means. To quantify theta coherence at different parts of the maze, the average theta coherence was calculated for three linearized maze sections that were determined upon visual inspection of **Figure 8c** (20-50 cm, 90-120 cm, 130-160 cm, **Figure 8d**).

Theta and gamma phase locking

HPC LFP data was Fourier transformed and filtered between 5-28 Hz and 40-100 Hz for theta and gamma oscillations, respectively. The filtered signal was Hilbert transformed to extract the theta and gamma phases. For every cell, the phases of HPC theta or gamma at which spikes occurred were extracted. The preferred firing phase ($\bar{a}$), mean vector length (MVL, r) and Rayleigh’s statistic were computed (Zar, 2010).

The rectangular coordinates of the preferred phase (X,Y) and the MVL were calculated with the equations below, where a_i denotes each phase and n the phase sample size:

$$X = \frac{\sum_{i=1}^{n} \cos a_i}{n} \ , \ Y = \frac{\sum_{i=1}^{n} \sin a_i}{n} \tag{2}$$

$$r = \sqrt{X^2 + Y^2} \tag{3}$$

Cartesian coordinates were converted back into polar coordinates:

$$\overline{a} = atan2\,(Y, X) \tag{4}$$

Finally, phases were wrapped onto 0 to 360 degrees. To test whether a cell is significantly locked to theta, the Rayleigh's test for circular uniformity was computed:

$$R = n * r \tag{5}$$

$$p = e^{\sqrt{1+4*n+4*(n^{2-R^2}) - (1+2*n)}} \tag{6}$$

A cell with a p value of < 0.05 was considered as significantly locked.

For mean MVL analysis in the different parts of the maze, the linearized maze was divided into start (10-50 cm), center (70-110 cm) and goal (130-170 cm). For a cell to get included in mean MVL calculation of a certain maze section, it had to fire a total of at least 30 spikes in that section over all trials in the respective block. The mean MVL was then computed as the mean of all the included cells' MVLs.

Analysis comparing the MVL of cells separately for pre-switch, switching and post-switch was performed for the maze center and for only those light rule trials with trajectories as during the spatial rule. The MVL of a cell for each of these three blocks was calculated with the same number of spikes (min_val). For a cell to be included in this analysis it had to have a total of at least 15 spikes in the center during the trials comprising each block. The block with the smallest number of spikes provided us with min_val. The MVL of a cell during a

block was computed 100 times with min_val randomly selected number of spikes occurring in that block. The MVL of a cell in a specific block was the median of these 100 computations.

To compare the MVL during correct and error trials during the rule-switching block, like above, only same trajectories were considered and the same number of spikes (i.e., 15) was used to calculate a cell's MVL during correct and error trials.

Linearized firing rate maps

The linearized 1D maze was divided into 20 spatial bins of 10 cm. Using the linearized position, an occupancy map was created by computing the amount of time the animal spent in each spatial bin during mobility periods (speed > 5 cm/s) (Dupret et al., 2010). For each cell the number of spikes fired in each spatial bin during mobility periods was counted, which was then divided by the occupancy time. These linearized vectors were then smoothed with a Gaussian filter with a SD of 1 bin.

Cofiring similarity

Spiking data of each cell was binned into 512 ms windows and only those periods were considered when the animal was in the center and had a speed of > 5 cm/s. Cofiring matrices (number of cells x number of cells) were generated by computing the scalar product of the binned spiking data of all possible cell pairs. The cofiring matrices of the following conditions were Pearson correlated: entirety of Rule 1 with Rule 2, first with last 12 trials of Rule1, first 12 trials of pre-switch with last 12 trials of post-switch, first with last 12 trials of Rule 2.

Cofiring flickering

Spiking data of each cell was binned into 512 ms windows and only those periods were considered where the animal was in the goal arm and had a speed of > 3 cm/s. Furthermore, for a given session only trajectory-matching trials were included. Cofiring matrices were computed for Rule 1 and Rule 2. Additionally, a cofiring matrix was generated for every trial (again, only taking trajectory-matching trials) of the pre-switch, switching and post-switch blocks. A trial's cofiring matrix was then Pearson correlated with that of Rule 1 and Rule 2, and the two correlation coefficients were subtracted from each other (correlation coefficient

Rule 2 minus correlation coefficient Rule 1). This value was then plotted as a vertical line in **Figure 13a,b**.

Place field similarity

A rate map is generated for every cell from all trials of a certain behavioral condition and the rate maps of all cells are stacked along the z-axis. The simultaneous activity of all cells in a particular spatial bin is the population vector for that particular set of coordinates. For every spatial bin, its population vector from one behavioral condition is correlated with the population vector of the other behavioral condition.

Bayesian decoding

The position of the animal was decoded using a Bayesian decoding algorithm on the spiking vectors of cells and their expected firing rate given by the rate maps (Zhang et al., 1998). Spiking neurons were assumed to follow a Poissonian law and act independently of each other. The position of the animal in a given time window of length τ is denoted as x. The number of spikes of one particular cell is denoted as σ_i , and the activity of all the cells considered in the given time window as $\bar{\sigma} = \{\sigma_1, \sigma_2, \ldots\}$. For each cell i and position x, we obtain the measured firing rate $\lambda_x{}^i$ from the rate maps. Using the assumptions and the introduced notation we have:

$$P(\bar{\sigma} \mid x) = \prod_i P(\sigma_i \mid x) = \prod_i Poiss(\sigma_i \mid \lambda_x{}^i \tau) \tag{7}$$

And, using the Bayesian rule:

$$P(x \mid \bar{\sigma}) = P(\bar{\sigma} \mid x) P(x) / P(\sigma) \tag{8}$$

For our computations we used a flat prior (i.e., $P(x)$ is uniform). The term $P(\sigma)$ does not need to be computed because one can enforce $\sum_x P(x \mid \bar{\sigma}) = 1$. The decoded position will then be:

$$BD(\bar{\sigma}) = argmax_x P(x \mid \bar{\sigma}) = argmax_x \prod_i Poiss(\sigma_i \mid \lambda_x{}^i \tau) \tag{9}$$

Cross-validation

The decoding quality of each ensemble was tested on rate maps constructed from data that was not used to train the model. For spatial coding analysis two thirds of the trials were used to compute the rate maps and the remaining third was used to decode the position of the animal during running periods. For analysis on non-local replay, rate maps were constructed from running (speed >5 cm/s) and immobility (speed <5 cm/s) periods and using all trials except for the one on which positional decoding was performed. For trajectory replay analysis during immobility periods, rate maps were constructed from running periods. The decoding error was the absolute value of the difference between recorded and decoded position.

Spiking window used for decoding

The spiking vector on which positional decoding is performed can be chosen in several ways. The standard way is to take spiking vectors with fixed time lengths. Another approach is to not fix the time, but instead select spiking vectors containing a minimum amount of spikes or a minimum number of spiking cells. We binned the spiking activity of each cell into time bins of 25.6 ms, thereby aligning it with the behavior tracking. The 25.6 ms spiking vectors were then summed up until the request of a certain time window length, number of spikes or number of cells participating was met. Unless otherwise stated, we used windows containing a fixed number of spikes ('Spiking-window'). Since the number and spatial properties of recorded cells differed for every recording session, the number of spikes contained in a window was selected for every session separately. This was done by computing the average decoding error during mobility (using the cross-validation method as described above) and determining the minimum number of spikes that allow positional decoding with a decoding error of less than 30 cm.

Confusion Matrix

The confusion matrix was computed as follows: given a vector of real positions rp and a vector of decoded positions dp with same length N, both binned into bins of 10 cm size, we initialized a 20 x 20 matrix (CM) to zero where rows corresponded to the real position and columns to the decoded position and filled it:

$$CM[i,j] = \sum_{k=0}^{N} (rp_k == i) \; and \; (dp_k == j) \tag{10}$$

Each row was then normalized so the sum of its elements equals 1.

Trajectory score

To ensure that the trajectories we observed during immobility were not only statistical noise of neurons, we computed a trajectory score, that consisted of a decoding probability and smoothness score. Each immobility period was divided into spiking-windows and, using the Bayesian algorithm, we obtained a probability density function on the binned linearized positions (i.e., decoding likelihood = vector with 20 entries with a sum of 1) for each spiking-window. Every 4 consecutive spiking-windows (i.e., the first three windows of a 4 spiking-window event will be the same as the last three windows of the previous event) that passed the continuity (no jumps > 6 bins) and speed (absolute speed > 20 cm/s) criteria were analyzed and forward and backward replaying trajectories were detected separately. The decoding probability score is a measure based on Xu et al., 2019. Starting from the first window of a 4-window event, we computed the probability of transitioning to the next with a velocity given by the slope of a line fitted on the four decoded positions. We multiplied the likelihood with a Gaussian kernel that moved by the corresponding amount of spatial bins to the left (backward) or to the right (forward). If the limit was reached (<0 or >20) the kernel was set to zero. We computed this measure for all windows of a 4-window event and averaged the result to obtain the decoding probability score that ranges between 0 (least optimal) and 1 (most optimal). The smoothness score measures how probable it is to find a permutation of the given event that has a distance between neighboring windows smaller than the original event. In the case of 4 or 5 windows, 24 or 120 permutations are possible. The number of permutations that had an average distance between neighboring events smaller than the real event, was divided by the total number of permutations, yielding a number from 0 (most optimal) to 1 (least optimal). For events longer than 5 windows, since it becomes computationally prohibitive to compute all the permutations, we randomly sampled 100 permutations and computed the score in the same way on those 100 samples. The smoothness score was then subtracted from the decoding probability score to obtain our final trajectory score, yielding a real number between -1 (least optimal) to 1 (most optimal) This way we penalized events that showed non-sequential activity.

Shuffling procedure

The probability that a 4-window (or longer) immobility period replays a trajectory was tested for significance by comparing it to trajectory scores obtained from a shuffled distribution. Trajectory scores were computed for every 4-window event like above, but this time 200 times using 200 shuffled rate maps. We employed a place field rotation shuffling, which, since we are using 1D rate maps, involves drawing a random integer between 3 and 17, and wrapping the rate map of each single neuron by that amount of bins around the origin.

Trajectory selection and concatenation

We selected all 4-window immobility events that had a unified trajectory score above the 95th percentile of their own shuffled distribution. Since replayed trajectories must not be limited to 4 windows but can be longer we incrementally extended significant 4-window events. A significant 4-window event was extended by the next 4-window event (which overlap by three windows), if the following conditions were met: the next 4-window event had to also have a significant trajectory score, the speed and jump sizes matched our criteria and the newly calculated trajectory score still passed the 95th percentile of its own shuffled distribution. The same procedure was then performed with the extended event.

Cross-correlation

Cross-correlation on HPC and mPFC trajectory replay events was performed to investigate their temporal alignment. For each brain area we considered a time series, aligned with behavior (25.6 ms), filled with zeros in case of immobility, ones for significant trajectory replay, and NaNs otherwise. The HPC time series was incrementally shifted to the left or right relative to the mPFC time series until a maximum of 20 bins. For each shift, a correlation between the two time series was computed excluding the NaNs (and thus mobility and non-task periods). To compare the cross-correlation to shuffled data, trajectory events were randomly shifted forward or backward within their immobility period 100 times, and each time a cross-correlation computed.

Trajectory replay and behavioral correlates

The immobility time in a trial or experimental block can vary slightly, depending on how long it takes for the animal to reach and consume the reward or to make a decision. We therefore computed a trajectory rate for every trial (i.e., number of trajectory replay events divided by the immobility time) instead of counting the number of trajectories per trial. We computed a trajectory rate separately for the center and goal area (i.e., at a linearized position of <110 cm or >110cm, respectively). For the center trajectory replay events were also divided into ahead and behind replaying trajectories. Depending on the analysis, an average rate was computed for every session from trials within the switching or within the switching and the post-switch block. When correlating the trajectory rate with the number of trials needed to switch to the new rule, we employed a logarithmic transformation of the trajectory rate. Insets in correlation figures show boxplots of 100 r-values computed from 100 correlations of randomly sampled data points from 80% of the data.

Statistics

Analyses were performed using custom written Python scripts. Non-parametric and two-tailed tests were used throughout. For paired comparisons Wilcoxon signed-rank test was used, whilst Mann-Whitney U test was used for unpaired data. For the analysis on trajectory replay in error and correct trials, the Wilcoxon signed-rank test was used and the multiple comparisons Bonferroni-Holm corrected. Correlations were performed by calculating the linear least-squares regression and the significance was determined using the Wald Test with t-distribution of the test statistic. For other multiple group testing the Kruskal-Wallis test was used. The 2-sample Kolmogorov-Smirnov test was used to compare distributions. A parametric 1-sample *t*-test tested for changes in firing rates.

RESULTS

Histology

We verified correct positioning of the recording tetrodes with cresyl violet-stained brain sections. **Figure 6** shows representative sections for the mPFC and HPC for each of the four rats. Tetrodes spanned the inner and outer cortical layers and thus data presented here included the activity from cells of all cortical layers.

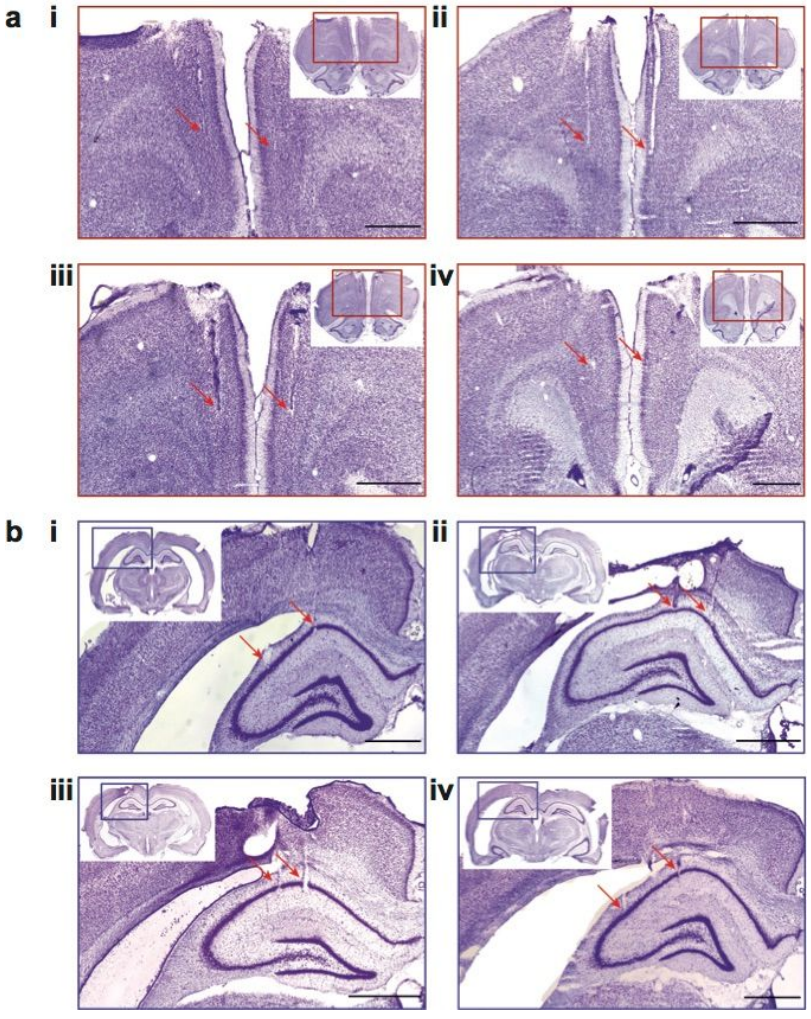

Figure 6: Histological verification of tetrode positioning in the mPFC and HPC.
Cresyl violet-stained coronal sections showing the tetrode tracks in the left and right Prl of the mPFC (**a**) and the right CA1 of the hippocampus (**b**). (**i**) rat jc189, (**ii**) rat jc190, (**iii**) rat jc196, (**iv**) rat jc200. Red arrows indicate tetrode tips. Scale bar denotes 1 mm.

Behavior

On each recording day the animal underwent behavioral blocks as follows: rest, remote rule 1 (remote recall), rest, pre-switch, switching, post-switch, rest, rule 2 (recent recall), and rest (**Figure 4a).** During rule 1 (remote recall) the last rule of the previous day applied. During pre-switch the animal had to again collect reward based on rule 1. Then the rule changed and reward had to be collected based on rule 2. Trials performed after the rule change, but before the animal reached good performance comprised the switching block. The beginning of good performance was defined as the center index after rule change where the error rate over five consecutive trials dropped to zero and marked the beginning of the post-switch block. Finally, during rule 2 (recent recall), the newly learnt rule applied. The animal had to perform cross-modal switches, i.e., switches from spatial to light or light to spatial rule, never between the two spatial rules (**Figure 4b**).

The unannounced change in rule lead to animals performing significantly more errors (n = 13 sessions; first 15 trials pre-switch vs. first 15 trials after rule change: P = 0.0014, Wilcoxon signed-rank test; **Figure 7**), but animals successfully updated to the new strategy in later trials (first 15 trials after rule change vs. last 15 trials of post-switch: P = 0.0014; **Figure 7**).

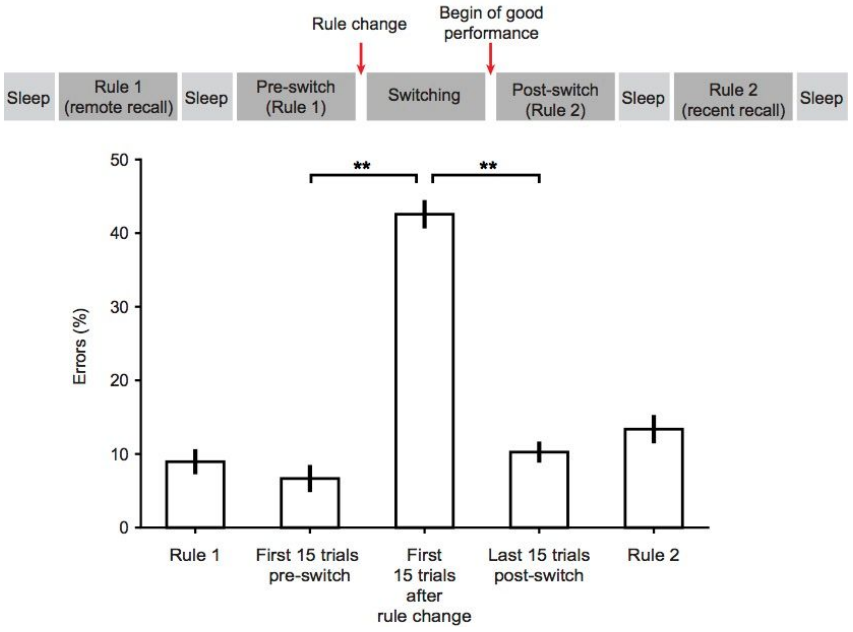

Figure 7: Increased errors after the rule change. The unannounced rule change lead animals to perform significantly more error trials, but animals eventually switched to the new strategy (**P <0.01, Kruskal Wallis Test).

Theta and gamma oscillations

Theta coherence

To investigate periods of increased information transfer between the HPC and mPFC, their theta coherence was computed. Since lesion studies demonstrated that the hippocampus and mPFC communicate ipsilaterally (Barker et al., 2017; Floresco et al., 1997; Navawongse and Eichenbaum, 2013), only right-hemisphere mPFC tetrodes were used for this analysis. Theta coherence between the HPC and ipsilateral mPFC was computed for each block, separately for recording sessions with a spatial-to-light and light-to-spatial rule switch. Mean theta coherence increased at the maze center for all blocks for both, spatial-to-light and light-to-spatial recording sessions (**Figure 8a,b**). Similarly, theta coherence was also increased at the goal compared to the start area. Since theta coherence in the two types of rule switches followed similar trends in the different blocks, coherence analysis was repeated over all the sessions, not separating by type of rule switch. This decreased the standard error, making the increase in theta coherence at the maze center to become more pronounced (**Figure 8c**). To quantify coherence values in different blocks and maze locations, the average theta coherence was computed for three 30 cm maze sections (**Figure 8d,e**). For all, but the pre-switch and rule 2 block, theta coherence in the center was significantly higher than that of the start (P (rule 1) = 0.022, P (pre-switch) = 0.22, P (switching) = 0.002, P (post-switch) = 0.002, P (rule 2) = 0.07, Mann-Whitney U test, Bonferroni-Holm correction). Similarly, for all but the pre-switch and rule 2 block, theta coherence was significantly higher in the goal than in the start (P (rule 1) = 0.016, P (pre-switch) = 0.34, P (switching) = 0.012, P (post-switch) = 0.016, P (rule 2) = 0.11, Mann-Whitney U test, Bonferroni-Holm correction). Although **Figure 8c** suggests that the increase in theta coherence at the center was highest during post-switch compared to blocks where the rule has not recently changed (rule 1, pre-switch, rule 2), maze center coherences were not significantly different (P = (rule 1 vs. post-switch) = 0.08, P (pre-switch vs. post-switch) = 0.09, P (post-switch vs. rule 2) = 0.07, Mann-Whitney U test, Bonferroni-Holm correction). However, the percentage increase in theta coherence in the center relative to the start was significantly higher in the post-switch than pre-switch block (P (post-switch vs. pre-switch) = 0.04, Mann-Whitney U test). In summary, theta coherence between the HPC and mPFC increases at maze locations associated with decision-making (center) and evaluation (goal). This was only seen for blocks associated with remote recall (rule 1) or

rule-switching (switching and post-switch blocks), suggesting that as cognitive demand increases so does HPC-mPFC theta interaction.

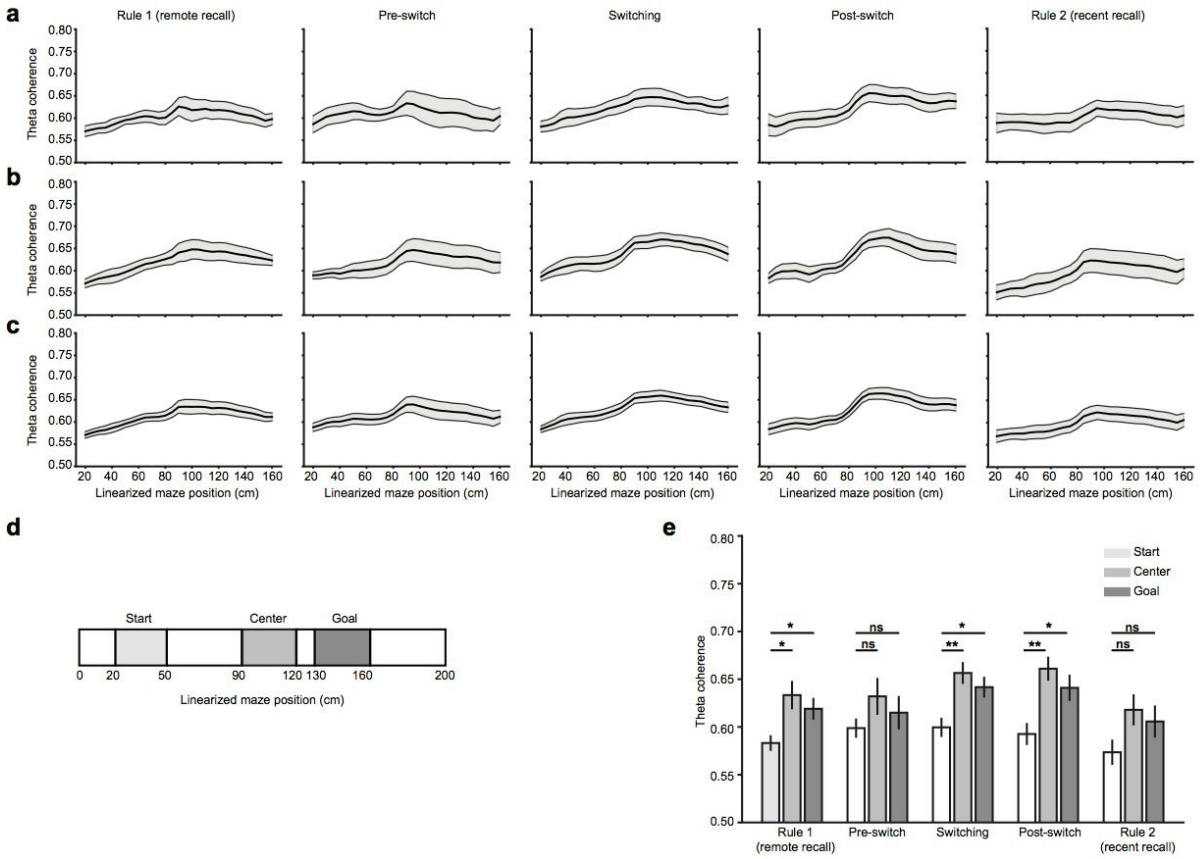

Figure 8: Increased HPC-mPFC theta coherence at maze center and goal.
(**a**) HPC-mPFC theta coherence computed over spatial-to-light rule sessions.
(**b**) HPC-mPFC theta coherence computed over light-to-spatial rule sessions.
(**c**) HPC-mPFC theta coherence computed over all sessions.
(**d**) Schematic of which parts of the linearized maze were taken to compute average coherence values for (e).
(**e**) Quantification of HPC-mPFC theta coherence computed over all sessions and separated for the start, center and goal of the maze. For all but the pre-switch and rule 2 block, theta coherence in the center and goal was significantly higher than in the start (*P <0.05, **P <0.01, ns - not significant, Mann-Whitney U test, Bonferroni-Holm correction).

Theta phase locking

To investigate phase locking to HPC theta oscillations, the mean phase, mean vector length (MVL) and Rayleigh's statistic were calculated for each cell. Similarly to the coherence analysis, mPFC phase-locking results were performed only on right-hemisphere mPFC cells.

Only putative pyramidal cells were used in the theta locking analysis (HPC: n = 1025 cells, right mPFC: n = 368 cells). A preferred phase histogram of significantly locked (Rayleigh's statistic $P < 0.05$) cells shows that HPC cells preferentially locked to the ascending phase of HPC theta, whilst mPFC cells preferentially locked to the descending phase (**Figure 9a**). Based on Rayleigh's statistic, 72% of HPC and 56% of mPFC cells were significantly locked. Next we calculated the MVL, a measure of how reliable a cell fires at one specific phase. Since the theta coherence results indicated that different parts of the maze are associated with different strengths of HPC-mPFC communication, the maze was divided into three sections, start, center and goal. Combining spatial-to-light and light-to-spatial sessions, the mean MVL was computed over all cells (not just significantly locked) for all task blocks (**Figure 9b**). In all task blocks HPC cells more strongly locked to HPC theta in the center (c) and goal (g) compared to the start (s) of the maze (rule 1: P(s vs. c) = 1.35e-10, P(s vs. g) = 2.18e-13; pre-switch: P(s vs. c) = 1.52e-13, P(s vs. g) = 2.00e-9; switching: P(s vs. c) = 8.00e-10, P(s vs. g) = 2.06e-7; post-switch: P(s vs. c) = 2.81e-11, P(s vs. g) = 1.67e-11; rule 2: P(s vs. c) = 1.71e-11, P(s vs. g) = 1.52e-9; Mann-Whitney U test, Bonferroni-Holm correction). mPFC cells showed smaller average MVL values than the HPC, but also phase locked most strongly to HPC theta in the center and goal area (rule 1: P(s vs. c) = 0.003, P(s vs. g) = 0.0003; pre-switch: P(s vs. c) = 0.0003, P(s vs. g) = 0.007; switching: P(s vs. c) = 0.001, P(s vs. g) = 0.0003; post-switch: P(s vs. c) = 1.92e-5, P(s vs. g) = 4.71e-5; rule 2: P(s vs. c) = 2.34e-6, P(s vs. g) = 1.62e-6, Mann-Whitney U test, Bonferroni-Holm correction).

We then investigated whether phase-locking strength differed with performance. For all trials of the rule-switch block (i.e., pre-switch, switching and post-switch), we calculated the MVL in the maze center during correct and error trials. For every cell, we ensured that the same number of spikes was used to calculate the MVL during correct and error trials (see Methods). We did not observe any differences in mPFC or HPC phase-locking strength to HPC theta oscillations between correct and error trials (HPC: P = 0.48; mPFC: P = 0.27, Mann-Whitney U test; **Figure 9c**).

To test for potential differences between the two rule types, MVL analysis was performed for the maze center during rule 1 (remote recall), separately for the spatial and light rule. Both, HPC and mPFC cells showed no differences in theta phase-locking strength between the two rules (HPC: P = 0.35; mPFC: P = 0.19, Mann-Whitney U test; **Figure 9d**). Similar results were obtained for the other blocks.

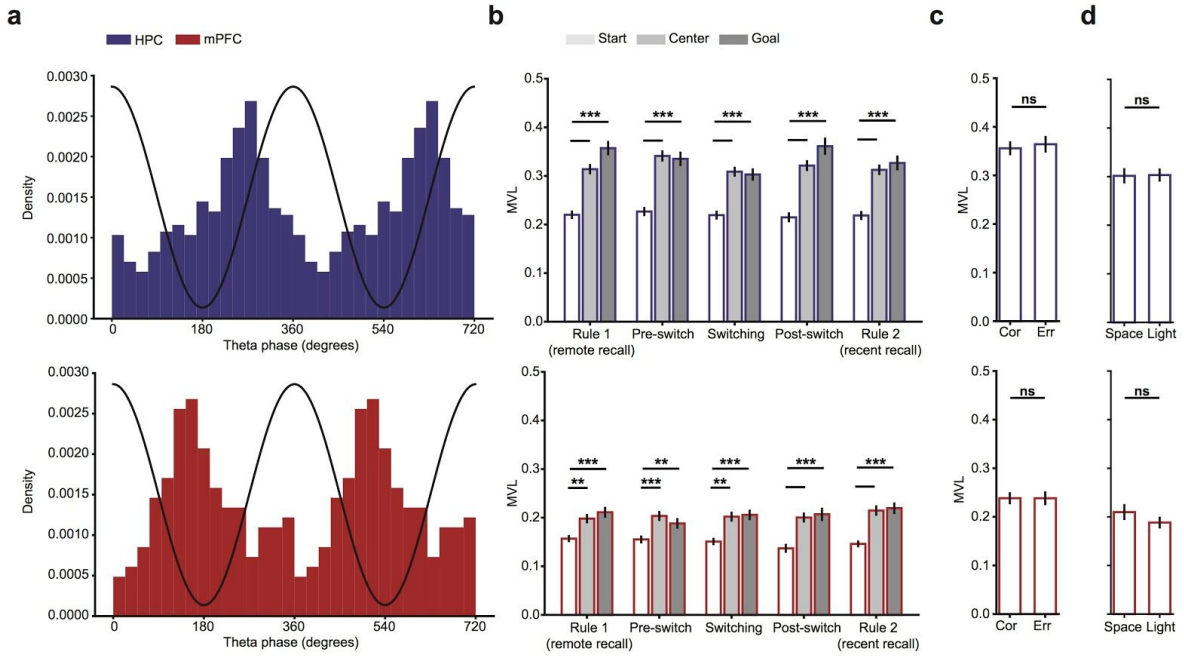

Figure 9: Increased theta phase locking strength of HPC and mPFC pyramidal cells at the maze center and goal.
(**a**) Preferred HPC theta oscillation phase of significantly locked HPC (top) and mPFC (bottom) cells. Black line illustrates two theta cycles.
(**b**) MVL of HPC (top) and mPFC (bottom) cells calculated over all sessions. The MVL of HPC and mPFC cells was higher in the center and goal, compared to the start of the maze.
(**c**) MVL did not differ between correct and error trials.
(**d**) MVL did not differ for the two different rule types. Here computed for the maze center during rule 1 (remote recall).
(*P <0.05, **P <0.01, ***P <0.001, ns - not significant, Mann-Whitney U test, Bonferroni-Holm correction).

Finally, to investigate whether mPFC theta phase-locking strength changes as a function of rule-switching, the MVL of mPFC cells was calculated separately for trials during pre-switch, switching and post-switch. This was done for the maze center and separately for sessions with a space-to-light and light-to-space rule switch. To compare activity during similar behaviors in the two rules, only those light rule trials that had trajectories matching those of that day's spatial rule were used for MVL calculation. Since MVL calculation is sensitive to the number of spike phases available, we ensured that the same number of spikes was used for calculating a cell's MVL for the three different blocks (see Methods). For **Figure 10a**, cells were first grouped into three groups, depending on whether their maximum MVL was during pre-switch, switching or post-switch, and then the cells were sorted within each group in descending order. Different groups of mPFC cells were maximally phase-locked during

different blocks. To quantify whether the type of rule switch (space-to-light or light-to-space) had an effect on the change in phase-locking strength between pre- and post-switch, we computed the absolute difference of pre- and post-switch MVL (i.e., |MVL(pre-switch) - MVL(post-switch)|), separately for the two types of rule switches. The average difference in phase-locking strength between pre- and post-switch did not differ for the two types of rule switches (P = 0.36, Mann-Whitney U test; **Figure 10c**). To investigate whether differences in MVL resulted from rule-switching or if MVL values also fluctuate during stable performance, we plotted the MVL of cells for the first and second half of rule 1 (remote recall) (**Figure 10b**). For **Figure 10b** cells were first grouped into two groups, depending on whether their maximum MVL was during the first or second half of the rule 1 (remote recall) block, and then the cells were sorted within each group in descending order. This also resulted in two groups of cells, each group showing stronger phase-locking for one half of the rule 1 (remote recall) block (**Figure 10b**). We then compared the mean MVL difference between pre- and post-switch (not separating for space-to-light and light-to-space rule switches) with that between the first and second half of rule 1 (remote recall). Unexpectedly, cells exhibited a greater phase-locking difference between first and second half of rule 1 (remote recall) than between pre-switch and post-switch (P = 0.0005, Mann-Whitney U test; **Figure 10d**). These results therefore do not suggest that mPFC cells code for rules with hippocampal theta phase.

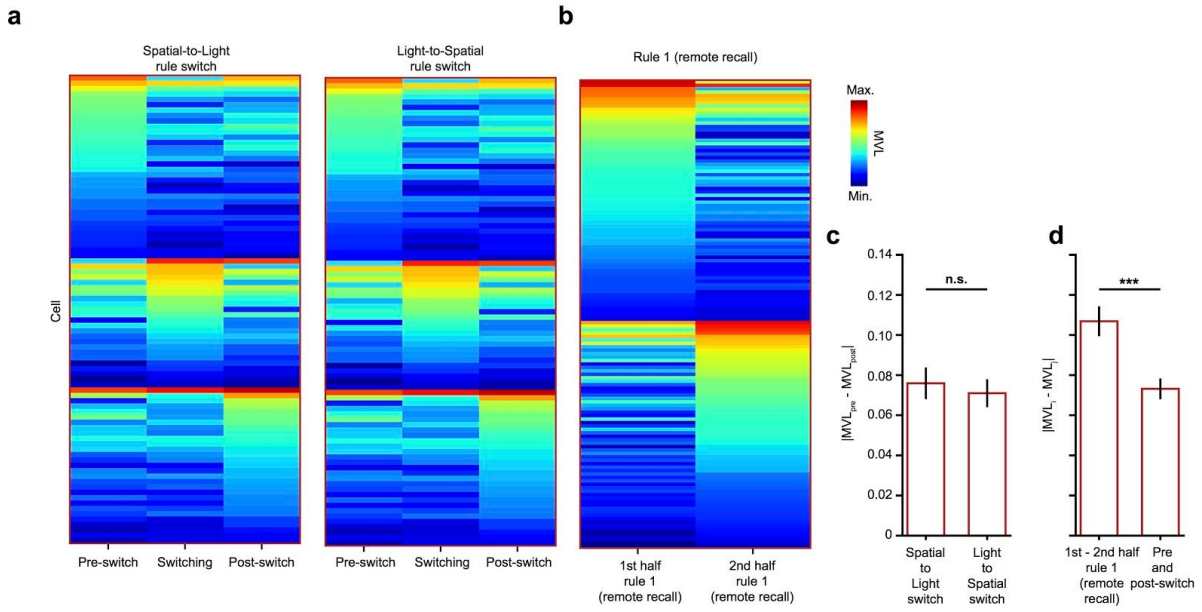

Figure 10: The theta MVL of mPFC cells does not code for rules.

(**a**) The MVL of mPFC cells during the pre-switch, switching and post-switch blocks, separately for sessions with a spatial-to-light (left) and light-to-spatial rule switch (right). The MVL is color-coded, warmer colors representing higher MVL. The left (space-to-light) and right (light-to-space) constitute different recording days and therefore the cell populations in these two figures are different. Sorting was done in the following way: Cells were grouped into three groups, depending on whether their highest MVL occurred during pre-switch, switching or post-switch. Cells in each group were then sorted in descending order of their MVL.

(**b**) The MVL of mPFC cells during the first and second half of rule 1 (remote recall) block. All sessions, and thereby rule types, are considered here. Cells were assigned into two groups, depending on whether their highest MVL occurred during the first or second half of rule 1 (remote recall). Cells in each group were then sorted in descending order of their MVL.

(**c**) The mean absolute difference between pre-switch and post-switch MVL, separately for space-to-light and light-to-space rule switch sessions. There was no significant difference, indicating that the MVL changes to a similar degree from pre- to post-switch, irrespective of the type of rule switch.

(**d**) The mean absolute difference between first and second half of rule 1 (remote recall) MVL and between pre- and post-switch MVL. All rule switch types are pooled together here. The MVL changed more between first and second half of rule 1 (remote recall) than between pre- and post-switch.

(***P <0.001, ns - not significant, Mann-Whitney U test).

Gamma phase locking

We next investigated phase locking to gamma oscillations and calculated the mean phase, mean vector length (MVL) and Rayleigh's statistic for each cell. Based on Rayleigh's

statistic, we found that only 8% of HPC and 5% of mPFC putative principal cells were significantly locked to HPC gamma oscillations. Combining spatial-to-light and light-to-spatial sessions, the mean MVL was computed over all cells (not just significantly locked) for all task blocks (**Figure 11a**). For all task blocks, the phase-locking strength of HPC cells to HPC gamma oscillations in the start was not different compared to that in the center or the goal (rule 1: P(s vs. c) = 0.25, P(s vs. g) = 0.09; pre-switch: P(s vs. c) = 0.19, P(s vs. g) = 0.056; switching: P(s vs. c) = 0.34, P(s vs. g) = 0.49; post-switch: P(s vs. c) = 0.28, P(s vs. g) = 0.41; rule 2: P(s vs. c) = 0.056, P(s vs. g) = 0.45; Mann-Whitney U test, Bonferroni-Holm correction). Similarly, for most task blocks, the phase-locking strength of mPFC cells to HPC gamma oscillations in the start was not different compared to that in the center or the goal (rule 1: P(s vs. c) = 0.08, P(s vs. g) = 0.27; pre-switch: P(s vs. c) = 0.32, P(s vs. g) = 0.44; switching: P(s vs. c) = 0.45, P(s vs. g) = 0.20; post-switch: P(s vs. c) = 0.024, P(s vs. g) = 0.16; rule 2: P(s vs. c) = 0.20, P(s vs. g) = 0.07; Mann-Whitney U test, Bonferroni-Holm correction). Only in the post-switch block was the gamma phase-locking strength of mPFC neurons stronger in the start compared to the center.

To investigate whether gamma phase-locking strength differed with performance, we calculated for all trials of the rule-switch block (i.e., pre-switch, switching and post-switch) the MVL in the maze center separately for correct and error trials. For every cell, we ensured that the same number of spikes was used to calculate the MVL during correct and error trials (see Methods). We did not observe any differences in mPFC or HPC phase-locking strength to HPC gamma oscillations between correct and error trials (HPC: P = 0.31; mPFC: P = 0.33, Mann-Whitney U test; **Figure 11b**).

To test for potential differences between the two rule types, gamma oscillation MVL analysis was performed for the maze center during rule 1 (remote recall), separately for the spatial and light rule. Both, HPC and mPFC cells showed no differences in gamma phase-locking strength between the two rules (HPC: P = 0.15; mPFC: P = 0.28, Mann-Whitney U test; **Figure 11c**).

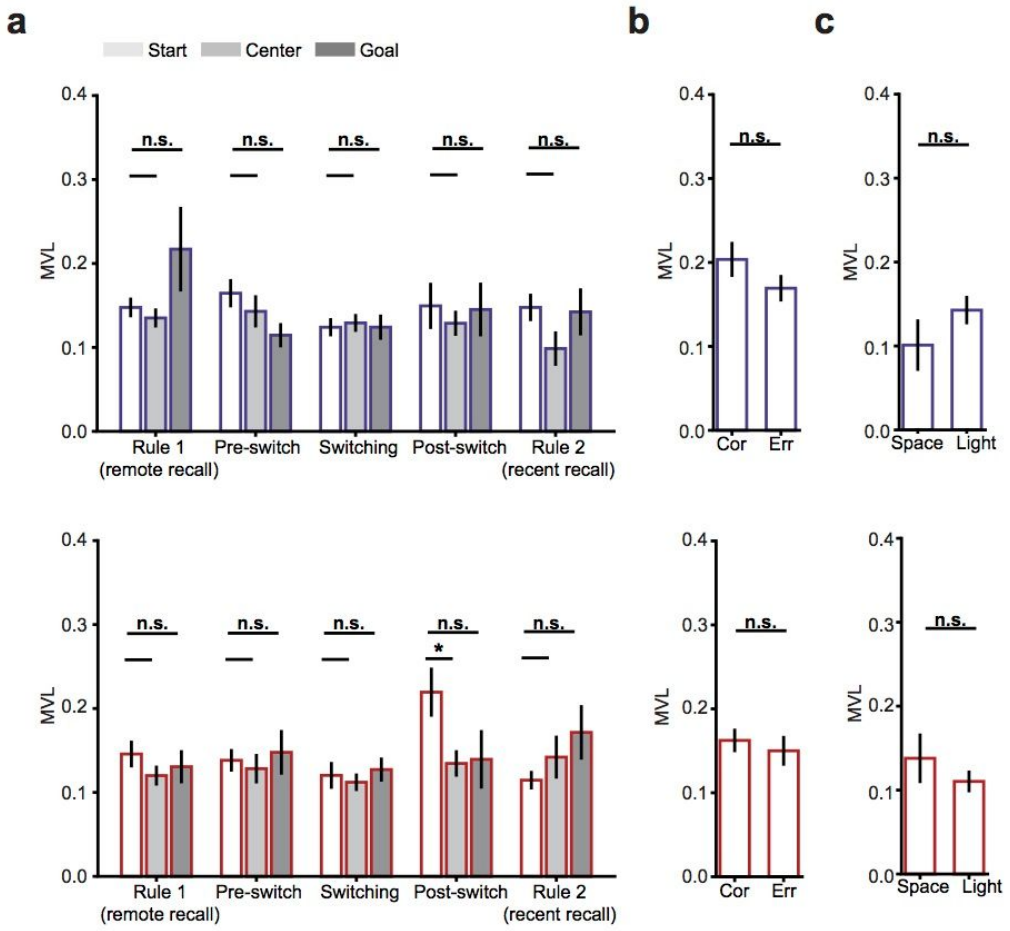

Figure 11: Gamma phase locking strength of HPC and mPFC pyramidal cells.
(**a**) MVL of HPC (top) and mPFC (bottom) cells calculated over all sessions. The MVL of HPC and mPFC cells did not differ in the start relative to the center or goal of the maze. Only in the post-switch block was mPFC phase-locking strength in the start higher than in the center or goal.
(**b**) MVL did not differ between correct and error trials.
(**c**) MVL did not differ for the two different rule types. Here computed for the maze center during rule 1 (remote recall).
(*P <0.05, ns - not significant, Mann-Whitney U test, Bonferroni-Holm correction).

Rule remapping

Cofiring similarity

To examine whether the activity of the HPC and mPFC codes for the rule, we analyzed cofiring dynamics between cell pairs. All putative HPC and mPFC pyramidal cells were included (HPC: n = 1025, mPFC: n = 817). Cofiring matrices were correlated between the following conditions: Rule 1 and Rule 2, first and last 12 trials of Rule 1, first 12 trials of pre-switch and last 12 trials of post-switch, first and last 12 trials of Rule 2. For the HPC, switching from one rule to another caused changes in cofiring dynamics as seen in the Rule 1 vs. Rule 2 cofiring matrix correlation (**Figure 12a,b**). That cofiring in the HPC changed as a result of the rule switch and not merely due to the passage of time is shown by the Pre- vs. Post-switch analysis. There, the Pre- vs. Post-switch correlation was lower than correlations from blocks with no rule change. For the mPFC, changes in cofiring dynamics with rule were only observed for Spatial-to-Light rule changes (**Figure 12c,d**).

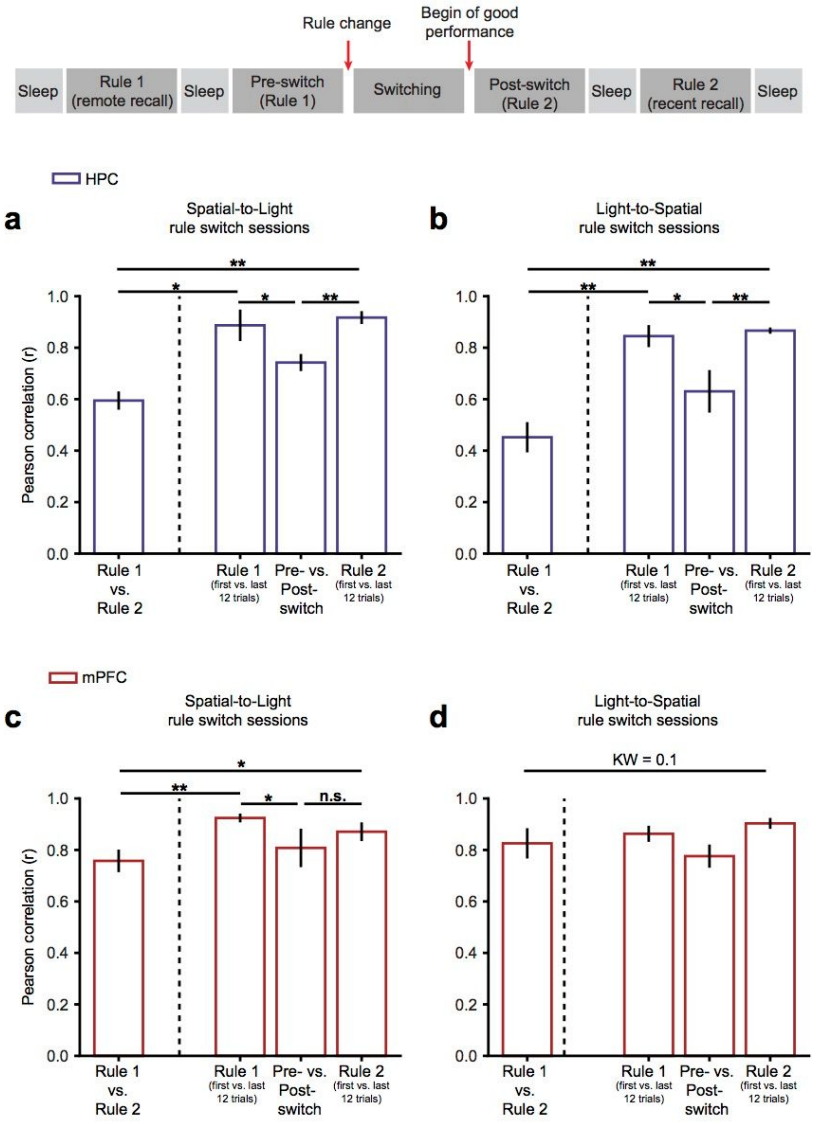

Figure 12: Cofiring dynamics and rule coding in the HPC and mPFC.

(**a**) Cofiring dynamics for HPC cell pairs in Spatial-to-Light rule switch sessions. In Rule 1 vs. Rule 2, cofiring matrices of the Rule 1 and Rule 2 blocks were correlated. In Rule 1, cofiring matrices of the first and last 12 trials of the Rule 1 block were correlated. In Pre- vs. Post-switch, cofiring matrices of the first 12 trials of pre-switch and last 12 trials post-switch block were correlated. Finally, in Rule 2, cofiring matrices of the first and last 12 trials of the Rule 2 block were correlated (Spatial-to-Light: P = 0.003, Kruskal Wallis Test; P (Rule 1 vs. Rule 2 - Rule 1 (first vs. last 12 trials)) = 0.02, P (Rule 1 vs. Rule 2 vs. Rule 2 (first vs. last 12 trials)) = 0.003, P (Pre- vs. Post-switch - Rule 1 (first vs. last 12 trials)) = 0.03, P (Pre- vs. Post-switch - Rule 2 (first vs. last 12 trials)) = 0.007, Mann-Whitney U post-hoc).

(**b**) Cofiring dynamics for HPC cell pairs in Light-to-Spatial rule switch sessions (Light-to-Spatial: P = 0.0007, Kruskal Wallis Test, P (Rule 1 vs. Rule 2 - Rule 1 (first vs. last 12 trials)) = 0.001, P (Rule 1 vs. Rule 2 - Rule 2 (first vs. last 12 trials)) = 0.001, P (Pre- vs. Post-switch - Rule 1 (first vs. last 12 trials)) = 0.02., P (Pre- vs. Post-switch - Rule 2 (first vs. last 12 trials)) = 0.004, Mann-Whitney U post-hoc).

(**c**) Cofiring dynamics for mPFC cell pairs in Spatial-to-Light rule switch sessions. (Spatial-to-Light: P = 0.02, Kruskal Wallis Test, P (Rule 1 vs. Rule 2 - Rule 1 (first vs. last 12 trials)) = 0.006, P (Rule 1 vs. Rule 2 - Rule 2 (first vs. last 12 trials)) = 0.02, (Pre- vs. Post-switch - Rule 1 (first vs. last 12 trials)) = 0.03, P (Pre- vs. Post-switch - Rule 2 (first vs. last 12 trials)) = 0.3, Mann-Whitney U post-hoc).
(**d**) Cofiring dynamics for mPFC cell pairs in Light-to-Spatial rule switch sessions (Light-to-Spatial: P = 0.1, Kruskal Wallis (KW) Test).
Data are expressed as mean ± s.e.m. Mann-Whitney U Test, $*P < 0.05$, $**P < 0.01$, $***P < 0.001$.

To illustrate the progression of changes in cofiring dynamics, we computed a cofiring matrix for every trial of the pre-switch, switching and post-switch block, but only including matching trajectories. A trial's cofiring matrix was correlated with the cofiring matrix of Rule 1 and Rule 2 (calculated for all matching trajectory trials). The correlation difference for every trial (correlation with Rule 2 minus correlation with Rule 1) is plotted in **Figure 13a**. Trials with a negative and positive correlation coefficient had cofiring patterns more similar to that of Rule 1 and Rule 2, respectively. Some trials after the rule change (vertical dashed line), HPC cofiring patterns become more similar to the Rule 2 block, indicating that HPC firing codes for rules. For the mPFC, however, cofiring similarity of trials varied without clear link to the rule change (**Figure 13b**).

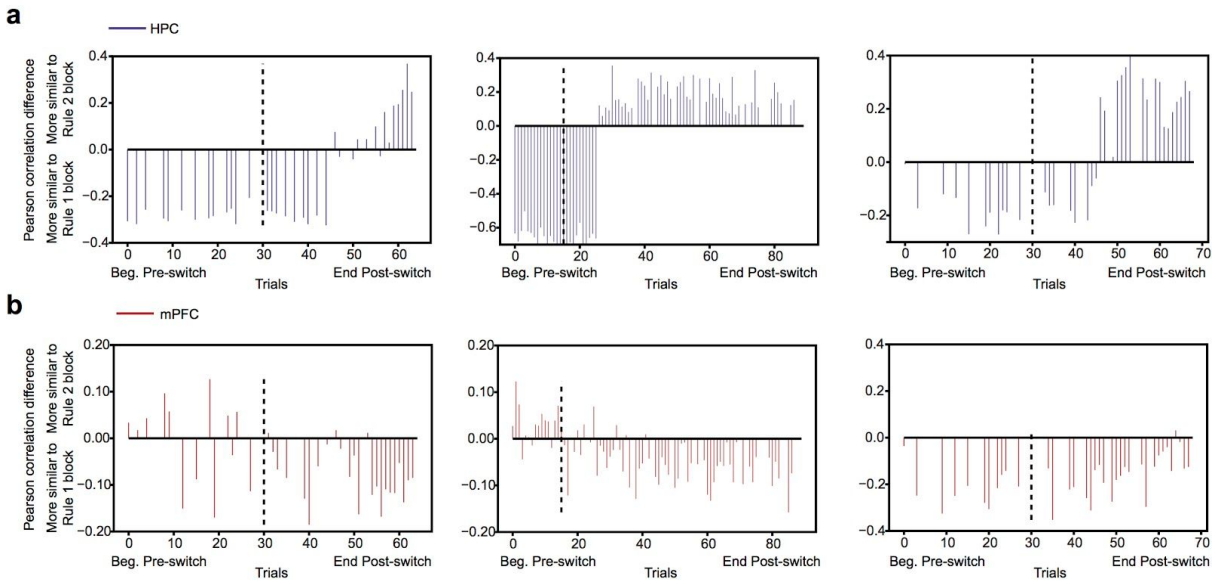

Figure 13: Trial-by-trial cofiring similarity to Rule 1 and Rule 2 blocks.
(**a**) Three example sessions illustrating how HPC cofiring changes with rule-switching. The cofiring matrix of a trial (within the pre-switch, switching and post-switch block) was correlated with that of the Rule 1 and Rule 2 block, and the two correlation coefficients were subtracted from each other and plotted as a vertical line. Negative and positive Pearson correlation differences indicate cofiring similarity with Rule 1 and Rule 2, respectively. The rule change (dashed vertical line) resulted in a different HPC cell pair cofiring configuration.
(**b**) The same three example sessions as above, but illustrating how mPFC cofiring changes with rule-switching. Cofiring matrix correlations were weaker than for the HPC. Furthermore, changes in mPFC cell pair cofiring were not related to the rule change (dashed vertical line) and for some sessions cofiring relationships became more similar to the Rule 1 block after the rule change.

Together with the results above, the mPFC seems to not code for rule types with cofiring relationships, or only does so for sessions with a Spatial to Light rule switch. Cofiring relationships in the HPC, however, differ for different rules.

Place field similarity

The place fields of hippocampal place cells can globally and rate remap upon changes to the environment (Leutgeb et al., 2005; Muller and Kubie, 1987). We therefore tested whether the spatial firing of HPC and mPFC cells undergoes rule switch-related remapping. Rate maps were correlated between the following conditions: Rule 1 and Rule 2, first and last 12 trials of Rule 1, first 12 trials of pre-switch and last 12 trials of post-switch, first and last 12 trials of Rule 2. For the HPC, the two rules were associated with different firing maps as seen in the Rule 1 vs. Rule 2, compared to the Rule 1 and Rule 2 rate map correlations (**Figure 14a,b**).

That remapping in the HPC was a result of the rule switch and not merely due to the passage of time is shown by the Pre- vs. Post-switch analysis. For Spatial-to-Light rule switch session, more remapping occurred between Pre- and Post-switch, than within Rule 1 or Rule 2. However, for Light-to-Spatial rule switch sessions, Pre- and Post-switch showed more remapping only compared to Rule 2, but not compared to Rule 1. For the mPFC during Spatial-to-Light rule switch sessions, the two rules were associated with different firing rate maps as seen in the Rule 1 vs. Rule 2, compared to the Rule 1 and Rule 2 rate map correlations (**Figure 14c**). Also, there was more remapping in the Pre- vs. Post-switch analysis, compared to within Rule 1 and Rule 2 (although Rule 2 only showed minimally less remapping than Pre- vs. Post-switch). In Light-to-Spatial rule switch sessions, the mPFC exhibited more remapping within Rule 1 than compared to the Rule 1 vs. Rule 2 or Pre- vs. Post-switch analysis (**Figure 14d**).

Taken together, the HPC seems to remap in response to a rule switch, however only for Spatial-to-Light rule switch sessions. Similarly for the mPFC, only in Spatial-to-Light rule switch sessions, did we observe rule switch-related remapping. However, there the rate maps within Rule 2 were only minimally more stable compared to the Pre- vs. Post-switch.

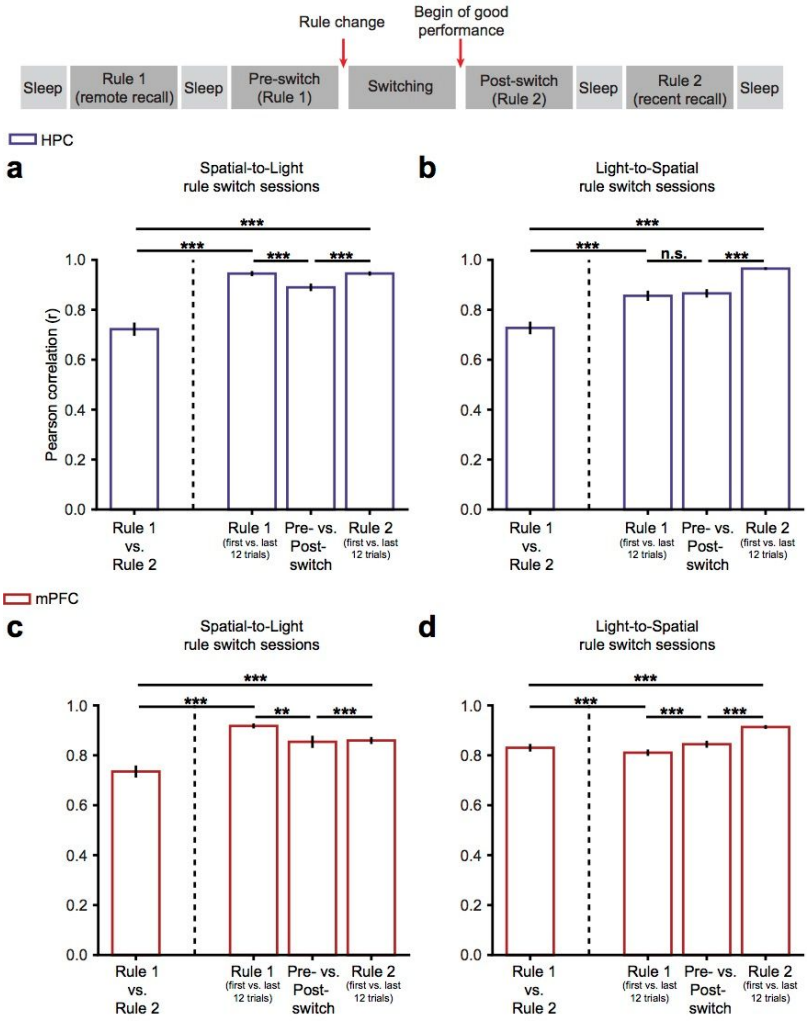

Figure 14: Remapping dynamics and rule coding in the HPC and mPFC.
(**a**) HPC rate map correlations for Spatial-to-Light rule switch sessions. In Rule 1 vs. Rule 2, rate maps of the Rule 1 block were correlated with rate maps of the Rule 2 block. In Rule 1, rate maps of the first 12 trials were correlated with rate maps of the last 12 trials of the Rule 1 block. In Pre- vs. Post-switch, rate maps of the first 12 trials of pre-switch were correlated with rate maps of the last 12 trials of post-switch. Finally, in Rule 2, rate maps of the first 12 trials were correlated with rate maps of the last 12 trials of the Rule 2 block. (Spatial-to-Light: P = 3e-72, Kruskal Wallis Test; P (Rule 1 vs. Rule 2 - Rule 1 (first vs. last 12 trials)) = 3e-49, P (Rule 1 vs. Rule 2 vs. Rule 2 (first vs. last 12 trials)) = 7e-50, P (Pre- vs. Post-switch - Rule 1 (first vs. last 12 trials)) = 9e-16, P (Pre- vs. Post-switch - Rule 2 (first vs. last 12 trials)) = 1e-13, Mann-Whitney U post-hoc).
(**b**) HPC rate map correlations for Light-to-Spatial rule switch sessions. (Light-to-Spatial: P = 6e-84, Kruskal Wallis Test, P (Rule 1 vs. Rule 2 - Rule 1 (first vs. last 12 trials)) = 8e-21, P (Rule 1 vs. Rule 2 - Rule 2 (first vs. last 12 trials)) = 8e-62, P (Pre- vs. Post-switch - Rule 1 (first vs. last 12 trials)) = 0.4, P (Pre- vs. Post-switch - Rule 2 (first vs. last 12 trials)) = 8e-40, Mann-Whitney U post-hoc).
(**c**) mPFC rate map correlations for Spatial-to-Light rule switch sessions. (Spatial-to-Light: P = 3e-50, Kruskal Wallis Test, P (Rule 1 vs. Rule 2 - Rule 1 (first vs. last 12 trials)) = 5e-45, P (Rule 1 vs. Rule 2 - Rule 2 (first vs. last 12 trials)) = 8e-21, (Pre- vs. Post-switch - Rule 1 (first vs. last 12 trials)) = 0.001, P (Pre- vs. Post-switch - Rule 2 (first vs. last 12 trials)) = 8e-5, Mann-Whitney U post-hoc).

(**d**) mPFC rate map correlations for Light-to-Spatial rule switch sessions. (Light-to-Spatial: P = 2e-35, Kruskal Wallis Test, P (Rule 1 vs. Rule 2 - Rule 1 (first vs. last 12 trials)) = 6e-4, P (Rule 1 vs. Rule 2 - Rule 2 (first vs. last 12 trials)) = 9e-24, (Pre- vs. Post-switch - Rule 1 (first vs. last 12 trials)) = 1e-5, P (Pre- vs. Post-switch - Rule 2 (first vs. last 12 trials)) = 1e-15, Mann-Whitney U post-hoc).

Trajectory replay

For the following analyses, only data from the pre-switch, switching and post-switch blocks were taken (**Figure 4a**). Furthermore, all putative HPC and mPFC pyramidal cells were included (HPC: n = 1025, mPFC: n = 817).

Spatial coding in the HPC and mPFC

We investigated place coding in the HPC and mPFC. **Figure 15** shows the firing rate of simultaneously recorded cells, i.e., from one recording session, along the linearized maze for the four different trajectories of the light-guided rule. HPC cells show spatially localized firing, where every part of the maze is coded for by a subset of cells. Albeit less selective, spatial firing was also seen for mPFC cells.

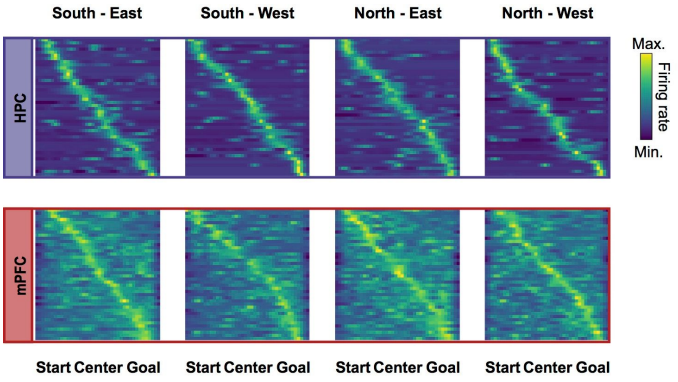

Figure 15: Spatial coding in the HPC and mPFC.
Linearized rate maps of HPC and mPFC cells for the four trajectories on the plus-maze. Simultaneously recorded cells from one example recording sessions are shown. Each rate map was normalized relative to the mean firing rate of a cell (Z-score). Cells are sorted based on the position of their peak firing rate.

To quantify spatial coding in the two areas, we employed a Bayesian algorithm on neuronal population firing to decode the position of the animal whilst running. Bayesian decoding was performed with a cross-validation procedure where rate maps were computed using two thirds of the running data and positional decoding was performed on the other third. When decoding the 2D position of the animal using the HPC cell population, the mean decoding error, i.e., the difference between the decoded and real spatial position, was 14 ± 1.3 cm ('2D decoding') (**Figure 16a**). This decoding error is similar to ones reported previously (Zhang et al., 1998). Decoding of the 2D position from the mPFC cell population, however,

yielded a large mean decoding error of 46 ± 3 cm (**Figure 16a**). We then constructed rate maps using the linearized position of the animal and hence decoded the animal's relative position between the start and goal, without distinguishing between the different arms ('1D decoding') (**Figure 16b**, bottom). Whilst 1D positional decoding using the HPC cell population did not alter the decoding precision (14 ± 1.3 cm; P = 0.5, Wilcoxon signed-rank test), the decoding precision improved strongly for the mPFC population (16 ± 3 cm; P = 0.0015, Wilcoxon signed-rank test). The 1D decoding performance using mPFC spiking was comparable to that of the HPC (P = 0.25, Wilcoxon signed-rank test). Since 1D decoding of mPFC and HPC spiking corresponded with the real position of the animal (**Figure 16c,d**), subsequent analyses were performed with linearized rate maps, where the two start and two goal arms are collapsed onto one map.

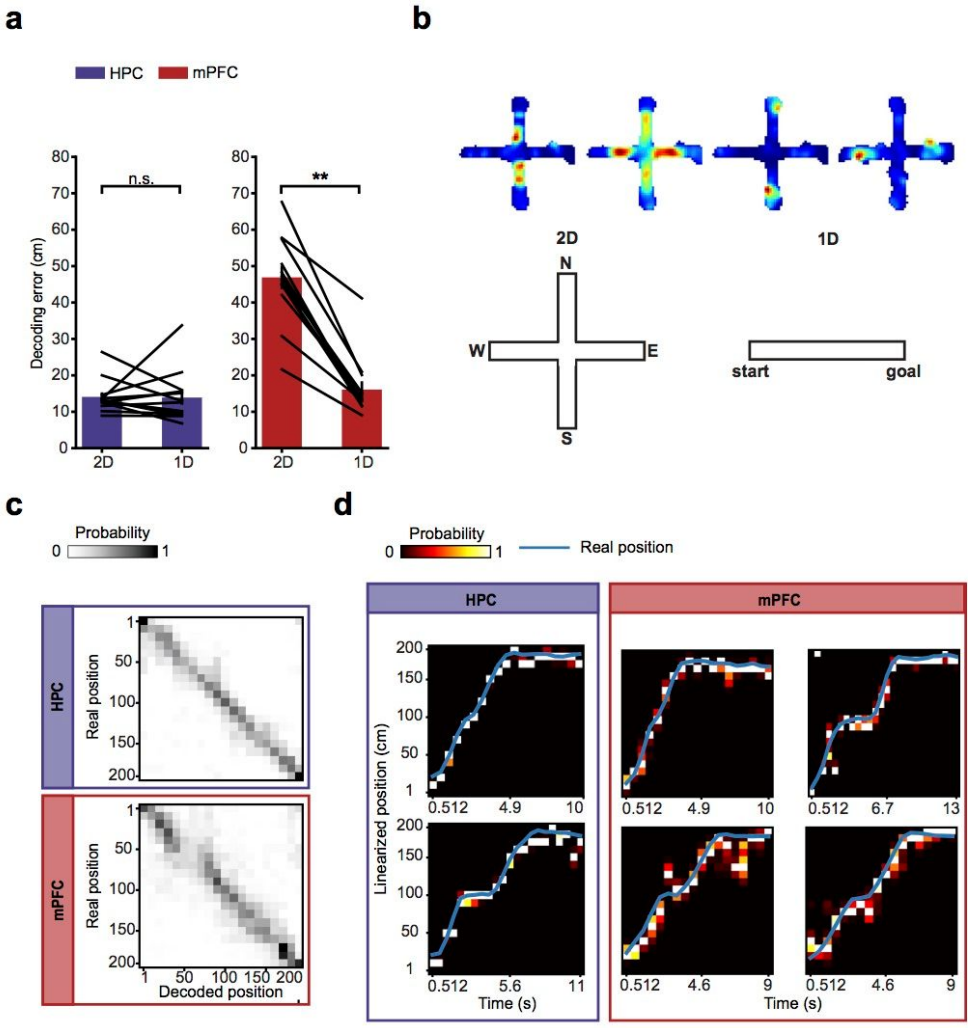

Figure 16: Spatial coding of the relative position in the mPFC.
(**a**) Mean decoding error for 2D and 1D positional decoding. Each black line represents one recording session. 1D positional decoding performed on mPFC population spiking lead to a strong improvement in decoding precision (***P* < 0.01, Wilcoxon signed-rank test).
(**b**) Examples of mPFC rate maps exemplifying the generalized coding of mPFC cells (top). Schematic of positions predicted with '2D' and '1D' decoding (bottom). When a mPFC cell has two place fields, in either both start or both goal arms, decoding the relative position between the start and the goal ('1D' decoding) with that cell's spiking information will lead to improved positional decoding performance.
(**c**) Confusion matrix for HPC and mPFC cell population. The diagonal indicates that there is a correspondence between the decoded and real position.
(**d**) 1D Bayesian decoding was performed on HPC (left) and mPFC (right) spiking for example trials. Position probabilities are plotted (black - low probability, white - high probability) with the rat's real position overlaid (blue line). Decoding was performed on time windows of 0.512 ms.

For the above analysis we binned spiking activity into time windows with a fixed length. However, spiking data can also be binned into windows of variable length, but containing a

minimum number of spikes or a minimum number of firing cells. We found that the number of spikes required to decode the position with a decoding error of less than 30 cm was lower for HPC cells ($P = 0.0014$, Wilcoxon signed-rank test; **Figure 17a**). The decoding error was plotted against windows of different number of spikes, windows with different number of firing cells and windows of different time lengths. Similar to the HPC, mPFC decoding error decreased with windows of increasing number of spikes, windows with increasing number of firing cells and windows of increasing time lengths, showing that the decoding performance improves with increasing information available (**Figure 17c**). Finally, for both the HPC and mPFC, the decoding errors in the pre-switch, switching and post-switch blocks did not differ (HPC: $P = 0.16$, mPFC: $P = 0.66$, Kruskal-Wallis-Test; **Figure 17b**).

In summary, these results suggest that, instead of coding for specific locations by distinguishing between the two start and goal arms, the mPFC holds information about the relative position between the start and the goal (**Figure 16b**), information likely required for goal-oriented navigation.

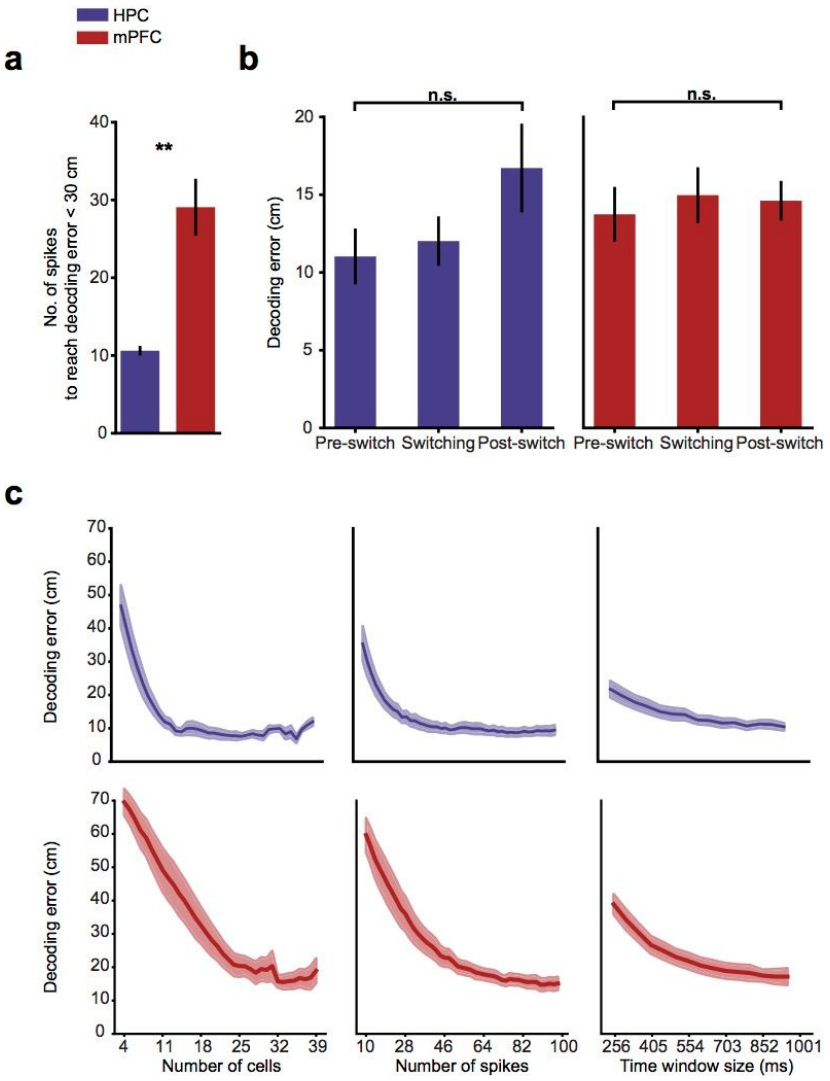

Figure 17: Positional decoding with HPC and mPFC spiking and its precision.
(**a**) The number of spikes to reach a decoding error of less than 30 cm was larger for the mPFC. Shown is the average over all sessions (**$P < 0.01$, Wilcoxon signed-rank test).
(**b**) Decoding performed with the HPC (left) and mPFC (right) population during the pre-switch, switching and post-switch block resulted in a similar decoding error (n.s. - non significant, Kruskal-Wallis-Test).
(**c**) Decoding error when performing Bayesian decoding on the HPC (top) and mPFC (bottom) population with windows containing an increasing number of firing cells, windows containing an increasing number of population spikes and windows of increasing duration. Positional decoding performed on HPC and mPFC spiking improved with increasing amount of information available.

Replay of non-local positions

During immobility the hippocampus has been shown to replay previously visited locations distant from the current position of the animal. To examine whether the mPFC shows similar

non-local (i.e., spatial locations not bound to the current position of the animal) reactivations, we decoded the position of the animal with mPFC population firing not only during running but also immobility periods (**Figure 18a,b**). Rate maps were computed including all trials except for the trial on which positional decoding was performed. Also, this time rate maps were computed without speed filtering in order to also have neural coding information for maze positions that are visited by the animal mainly during immobility. This procedure therefore ensured that any non-local position decoded from mPFC spiking recorded during immobility did not result from a lack of encoding information during immobility. We found that the position encoded by the mPFC population can be highly non-local. The distribution of decoding errors during immobility periods showed two peaks, with the highest peak at zero and a second, smaller one, at ~150 cm away from the real location (**Figure 18b**). The majority of non-local events occurred during immobility (**Figure 18c**).

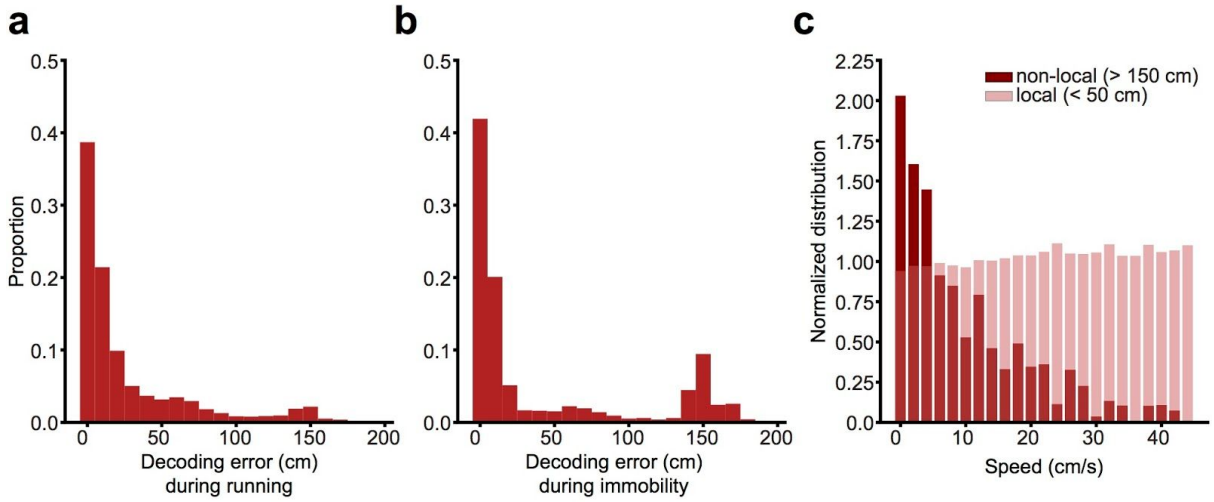

Figure 18: During immobility the mPFC encodes non-local positions.
(**a**) The distribution of decoding errors when positional decoding was performed on mPFC spiking data that was recorded during running periods.
(**b**) The distribution of decoding errors when positional decoding was performed on mPFC spiking data that was recorded during immobility periods. Note the increased occurrence of decoding errors of ~150 cm, indicating that during immobility the mPFC increasingly reactivates positions distant from the animal's actual location.
(**c**) Distribution of the animals' speed for local (decoding error of < 50 cm) and non-local (decoding error of > 150 cm) activity events in the mPFC. Note that most non-local events occur at low speeds when the animal is immobile.

Replay of trajectories in the mPFC

The hippocampus can reactivate entire past or future trajectories serving cognitive functions such as memory consolidation and future planning (Csicsvari et al., 2007; Davidson et al., 2009; Diba and Buzsáki, 2007; Foster and Wilson, 2006). Similar temporally-organized replay has also been reported for the visual cortex and medial entorhinal cortex (Ji and Wilson, 2007; O'Neill et al., 2017). During immobility the mPFC represented locations away from the animal's actual position (**Figure 18**). We therefore tested whether the mPFC links individual non-local positions to an ordered sequence of locations, thereby recapitulating an extended behavioral experience. For each session and separately for HPC and mPFC, we selected the number of spikes that allowed us to decode the position of the animal during running with an average error lower than 30 cm. Immobility periods were then divided into these spiking-windows that contained the same number of spikes (Stella et al., 2019). Using the Bayesian position-decoding algorithm and rate maps computed from spiking activity during running periods, a probability density function on the binned linearized positions was computed for each spiking-window. For every event of 4 consecutive spiking-windows a trajectory score was computed, based on the decoding probability between decoded positions (decoding probability score) and the smoothness of the trajectory (smoothness score). The decoding probability score represents an average of the probabilities of transitioning from the decoded position in one window to the next at a certain speed and ranges between 0 (least optimal) and 1 (most optimal). The smoothness score measures how many permutations of the given event show a smaller average jump between neighboring windows than the original event. This score ranges between 0 (most optimal) and 1 (least optimal) and is used as a penalization. We allowed both forward and reverse-replaying trajectories with a replay speed of at least 20 cm/s, and excluded trajectories where jumps between neighboring spiking-windows were bigger than 60 cm. Both scores were tested against chance using a place field rotation shuffling procedure. The shuffling was executed 200 times independently for each 4 spiking-window event, yielding a distribution of shuffled scores that we tested our results against. We observed that the decoding probability score distributions were significantly different, with scores closer to zero for shuffled events ($P < 0.00001$, 2-sample Kolmogorov-Smirnov (KS) test; **Figure 19a**). The difference remained significant when taking 4 spiking-window events that do not overlap with other 4 spiking-window events ($P < 0.00001$, 2-sample KS test; **Figure 20a**). The smoothness score distributions were also significantly different and were higher for the shuffled events ($P < 0.00001$, 2-sample KS test; **Figure 19b**). We unified the two measures

by subtracting the smoothness score from the decoding probability score, yielding the trajectory score, a real number ranging between -1 (least optimal) to 1 (most optimal). 4-window events that had a unified score above the 95th percentile of their own shuffled distribution were then identified as significant trajectory events and selected. Since replayed trajectories can be longer than 4 spiking-windows, significant 4-window events were incrementally extended in the following way: for a significant 4-window event, if the following (overlapping by three windows) 4-window event was also significant, it was extended by that event, if the speed and jump sizes matched our criteria and the newly calculated trajectory score still passed the 95th percentile of its own shuffled distribution. This resulted in 58% and 60% of the considered 5-window events in the HPC and mPFC, respectively, to pass their own shuffled distribution (both $P < 0.00001$, Binomial Test). The same procedure was then performed with the extended event.

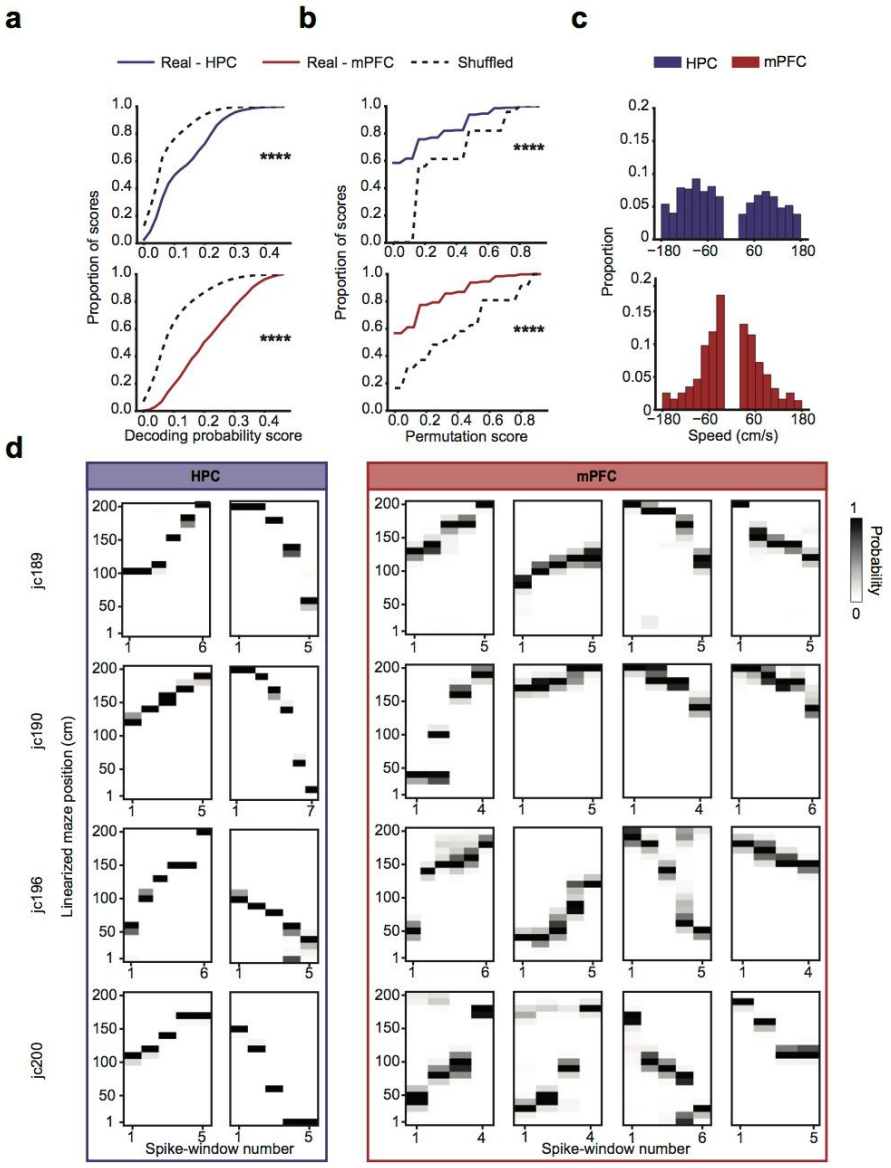

Figure 19: Replay of trajectories in the mPFC during immobility.

(**a**) The cumulative distribution of decoding probability scores computed from real and place field-rotated shuffled data. For the HPC (top) and mPFC (bottom), the decoding probability scores of the real data were significantly higher than of the shuffled data (****P <0.00001, 2-sample KS test).

(**b**) The cumulative distribution of smoothness scores computed from real and place field-rotated shuffled data. For the HPC (top) and mPFC (bottom), the smoothness scores of the real data were significantly lower than that of the shuffled distribution (****P <0.00001, 2-sample KS test).

(**c**) Distribution of the speed of trajectory replay occurring in the HPC (top) and mPFC (bottom). One criterion for an event to replay a trajectory was a reactivation speed of above 20 cm/s. Depending on whether an event replays a trajectory in the forward or reverse order it will have a positive or negative speed, respectively.

(**d**) Examples of trajectory replay events in the HPC (left) and mPFC (right) for all rats. Decoding was performed on windows with a fixed number of spikes (i.e., spike-window) and the position probabilities plotted for all maze positions. For the HPC, the first column shows

forward and the second column reverse replay. For the mPFC, the first two columns show forward and the last two columns reverse replay.

As a control, to further verify the validity of longer than 4-window events, we computed the decoding probability and smoothness scores for 5 and 6 spiking-window events, with overlapping windows as described above. We observed that the distributions of decoding probability and smoothness scores were still significantly different from chance (decoding probability score: HPC and mPFC all P <0.00001, smoothness score: HPC and mPFC all P <0.00001, 2-sample KS test; **Figure 20b-e**).

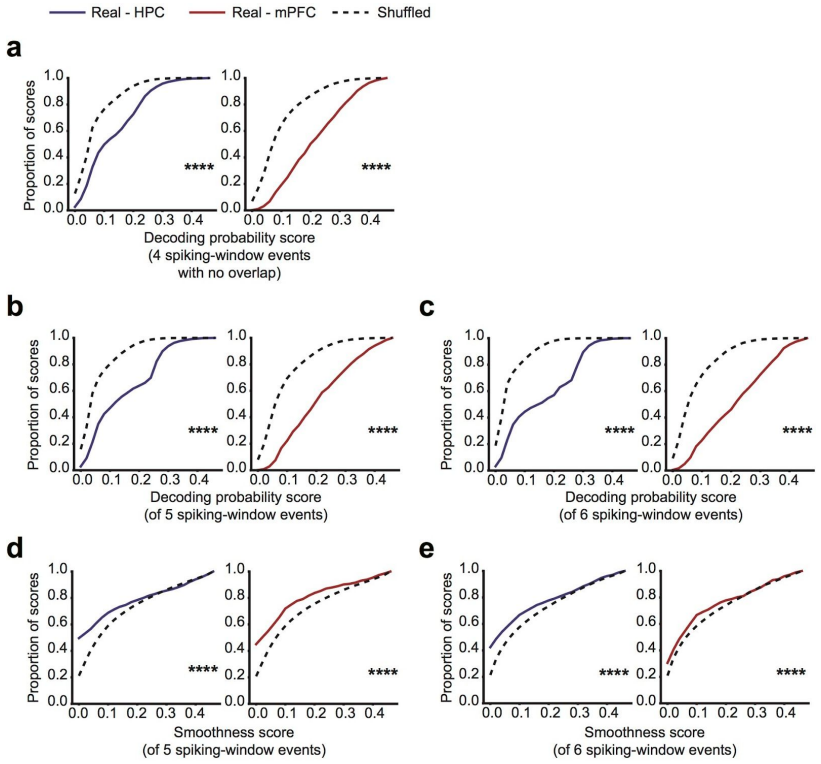

Figure 20. Alternative selection of trajectory events and their distributions of scores.
(**a**) The distribution of decoding probability scores was still significantly different from chance when 4 spiking-window events were non-overlapping.
(**b**) The distribution of decoding probability scores was still significantly different from chance for 5 (instead of 4) spiking-window events.
(**c**) The distribution of decoding probability scores was still significantly different from chance for 6 (instead of 4) spiking-window events.
(**d**) The distribution of smoothness scores was still significantly different from chance for 5 (instead of 4) spiking-window events.
(**e**) The distribution of smoothness scores was still significantly different from chance for 6 (instead of 4) spiking-window events (****P <0.00001, 2-sample KS test).

All together, 9% of the time spent immobile showed significant mPFC trajectories. Selected mPFC events resembled trajectories typically seen in the HPC (**Figure 19d**). The duration of trajectory replay events in mPFC was longer than in the HPC (median, mPFC: 0.74 s, HPC: 0.33 s; $P < 0.00001$, Mann-Whitney U test). The distribution of trajectory replay speeds was wider in HPC than mPFC (95th confidence intervals, cm/s: HPC: [-491, 452], mPFC: [-186, 191]), and both showed forward and reverse-playing trajectories (**Figure 19c,d**). The rasterplot in **Figure 21** illustrates that during mPFC trajectory replay events, a sudden change in network activity occurs, which is typically also seen for HPC replay events.

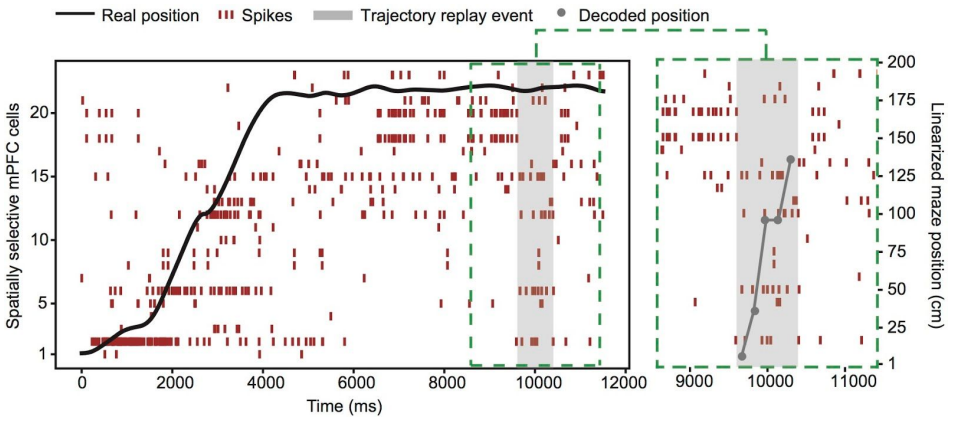

Figure 21: Sudden change in mPFC network activity during a trajectory replay event. Spiking of spatially-selective mPFC cells (spatial information > 0.1, sparsity < 0.1) during an example trial. The black line denotes the real position of the rat and the grey shaded area an event where trajectory replay has been detected. The dashed green box zooms into the trajectory replay event. Note the change in network activity (i.e., increase or decrease in firing rate) during the trajectory replay event.

We then performed a cross-correlation between the occurrence of significant trajectory replay events in the HPC with those in the mPFC and found that trajectory replay in these two areas was independent of each other (**Figure 22a**). However, the speed of trajectory replay in both areas was correlated with the population firing rate in the corresponding area ($P < 0.00001$, 1-sample *t*-test; **Figure 22b**).

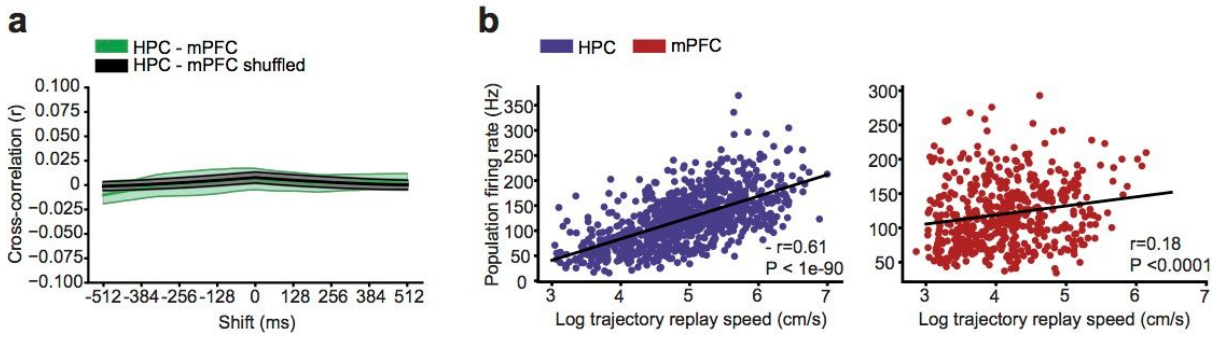

Figure 22: HPC and mPFC trajectory replay events do not co-occur.
(**a**) Cross-correlation of trajectory replay events detected in the HPC and mPFC. The cross-correlation did not show any peaks and overlapped with that of the shuffled data, indicating that trajectory replay events in these two areas generally do not co-occur.
(**b**) For both the HPC and mPFC, the population firing rate positively correlates with the trajectory event replay speed (1-sample *t*-test).

Trajectory replay in the mPFC correlates with rule-switching performance

SWR-associated awake replay in the hippocampus has been proposed to support spatial task performance (Jadhav et al., 2012; Singer et al., 2013). To investigate whether awake trajectory replay in the mPFC goes beyond a mere recapitulation of experience to possibly supporting the mPFC's role in rule-switching, we studied the relationship of awake trajectory replay with rule-switching performance. We calculated a rate of trajectory replay by dividing the number of trajectory replay events in a trial by that trial's immobility time. Then, the mean trajectory rate in the switching block was plotted against the number of trials required to switch to the new rule. Trajectory replay rate in the maze center of neither brain area correlated with performance (HPC: r = 0.41, P = 0.27; mPFC: r = -0.55, P = 0.1; **Figure 23a**). However, the rate of mPFC trajectory replay events at the goal negatively correlated with the number of trials required to switch to the new rule and hence positively correlated with performance (r = -0.66, P = 0.01; **Figure 23b**). Conversely, HPC trajectory replay in the goal area positively correlated with number of trials to switch and hence showed a negative correlation with performance (r = 0.61, P = 0.04; **Figure 23b**).

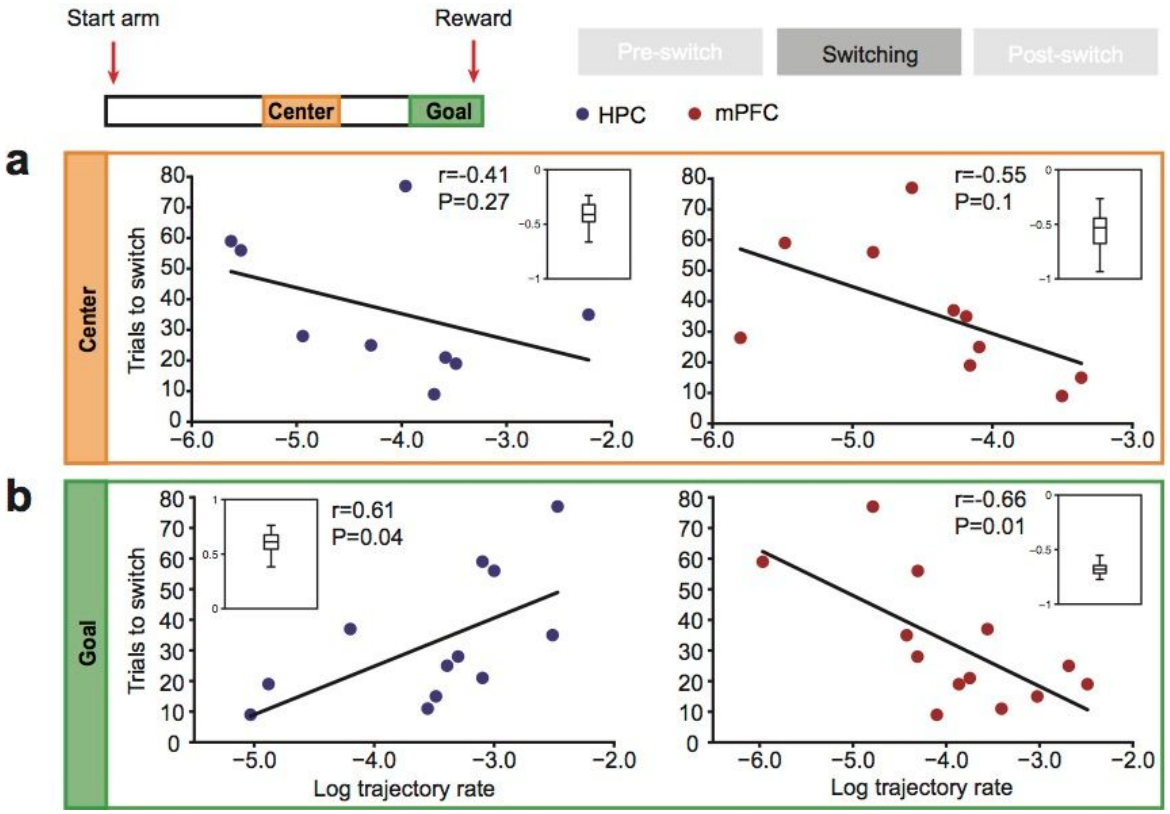

Figure 23: HPC and mPFC trajectory replay and rule-switching performance.
A mean trajectory replay rate was calculated for switching block trials.
(**a**) The trajectory replay rate in the maze center for the HPC (left) and mPFC (right) did not correlate with number of trials required to switch to the new rule. Inset shows mean r-value obtained from 100 correlations of bootstrapped data. Each dot denotes one session and sessions with no trajectory replay for a condition were excluded.
(**b**) The trajectory replay rate at the goal for the HPC (left) positively correlated with the number of trials required to switch (i.e., negatively correlated with performance). Conversely, the trajectory replay rate at the goal for the mPFC negatively correlated with the number of trials required to switch (i.e., positively correlated with performance).

We then computed the mean trajectory rate separately for correct and error trials over all trials after the rule switch (i.e., trials from the switching and post-switch block). The mPFC trajectory replay event rate at the goal was higher in error than correct trials (P = 0.009, Wilcoxon signed-rank test; **Figure 24b**). This result, together with the positive correlation with performance, provides support that mPFC trajectory replay at the goal area during error trials might facilitate switching to the new rule. For the HPC, goal trajectory replay was slightly increased in error trials (P = 0.016, Wilcoxon signed-rank test; **Figure 24b**). HPC trajectory replay in the center was higher during correct than in error trials, also when separating for decoded trajectories ending ahead and behind the animal (total: P = 0.0015, ahead: P = 0.006, behind: P = 0.02, Wilcoxon signed-rank test, Bonferroni-Holm correction;

Figure 24a,c). This result fits with previous reports that the hippocampus shows more coordinated replay preceding correct than error trials (Singer et al., 2013). Separating ahead and behind trajectory replays in the center for the mPFC showed that whilst there were more ahead trajectories during error trials, there were more behind trajectories during correct trials (total: P = 0.05, ahead: P = 0.006, behind: P = 0.003, Wilcoxon signed-rank test, Bonferroni-Holm correction; **Figure 24a,c**), suggesting that ahead and behind trajectories in the mPFC might serve different functions.

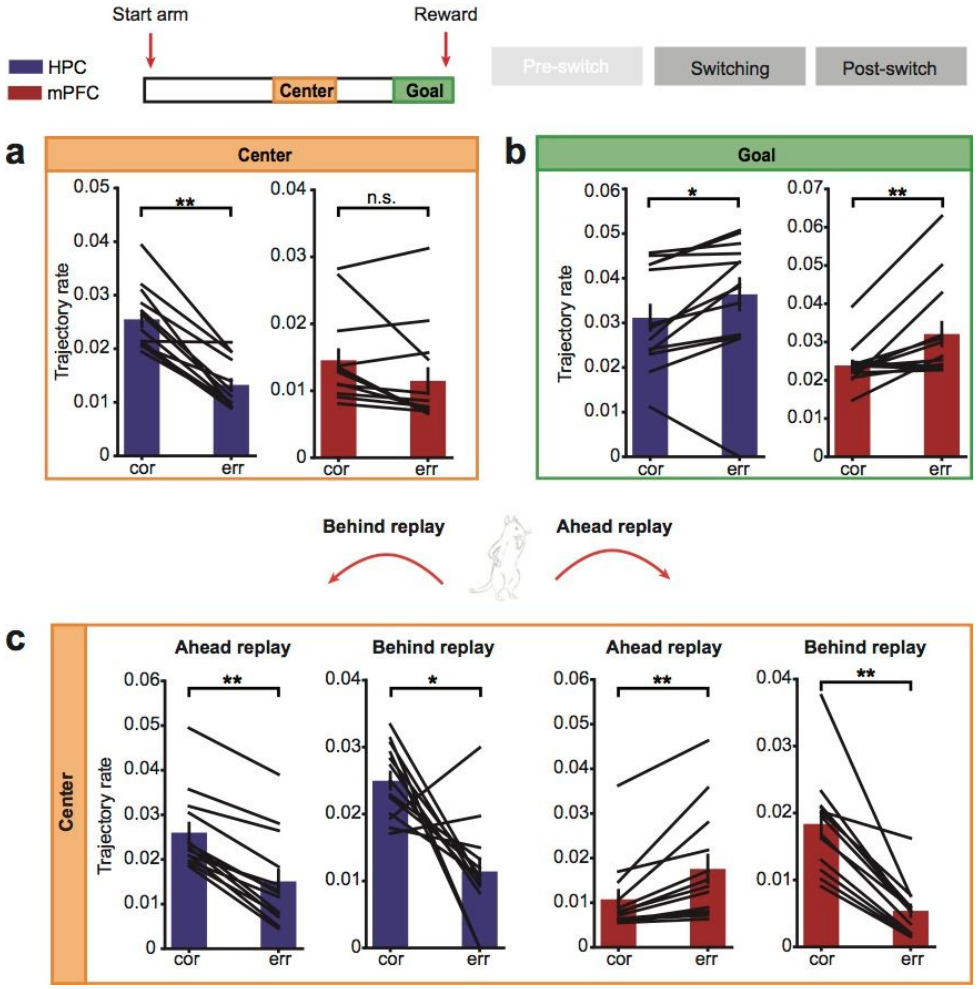

Figure 24: Trajectory replay in correct and error trials.
A mean trajectory replay rate was calculated for switching and post-switch block trials.
(**a**) HPC trajectory replay rate in the center was higher during correct than error trials.
(**b**) Trajectory replay rate at the goal was higher during error than correct trials for both the HPC and mPFC.
(**c**) Separating replay events in the center into ahead and behind replaying trajectories, showed that for the mPFC ahead replay was increased during error trials, whilst behind replay was increased during correct trials. Ahead and behind trajectory replay in the HPC did not seem to support different functions and were both increased at correct trials.
(*P < 0.05, **P < 0.01, Wilcoxon signed-rank test).

DISCUSSION

Theta and gamma oscillations

Our results showed that theta coherence between the HPC and mPFC was increased in the maze center and goal relative to the start during most task blocks. Similarly, phase locking strength of HPC and mPFC cells to HPC theta was increased in the center and goal compared to the start for all task blocks. However, no difference in theta coherence or phase locking strength was seen for the two different rules. Furthermore, the phase locking strength of mPFC cells to HPC theta can change over trials and is not related to a switch in strategy. Finally, phase locking strength of HPC and mPFC cells to HPC gamma oscillations was similar for the different parts of the maze and did not differ between the different rules.

Oscillatory coherence is thought to facilitate precise temporal coordination and information transfer between brain regions (Buzsáki and Draguhn, 2004; Fries, 2005). Phase locking strength is a related measure and is also associated with increased coding fidelity. Increased phase locking strength of mPFC to hippocampal theta indicates increased interaction between these two areas. Both measures have been shown to be increased at task stages that have higher cognitive demand (Benchenane et al., 2010; Jones and Wilson, 2005). Similar to previous studies, we found increased HPC-mPFC theta coherence and mPFC phase locking at the maze decision point and goal area. What information might be shared between the hippocampus and mPFC during these moments? Before the animal makes a decision to turn, the current rule has to be retrieved and the appropriate response selected. The mPFC might hold information about the rule that aids the hippocampus to correctly navigate, information that might be shared via oscillatory mechanisms. Indeed, directionality of theta amplitude cross-correlation was directed from the hippocampus to mPFC during contextual retrieval and from the mPFC to hippocampus during retrieval of context-appropriate hippocampal memory, indicating transfer of information between these two areas (Place et al., 2016). At the goal the choice has to then be evaluated and the memory of the reward place reinforced. These functions might be subserved by the hippocampus and mPFC, since mPFC is modified by errors (Narayanan and Laubach, 2008) and hippocampal-cortical interactions underlie memory consolidation (Maingret et al., 2016). Coherence has been reported to be particularly high after a rule switch (Benchenane et al., 2010), however, in our data the slightly larger increase in mean theta coherence and

decrease in variability in post- compared to pre-switch seen in **Figure 8c** was not significant (**Figure 8e**). Coherence was increased in the center and goal compared to the start for most task-blocks and not just during post-switch. Since all animals performed the rule-switching task for a maximum of five days it is possible that with increasing task familiarity, coherence will decrease during blocks with no rule-switching. We could also not confirm previous links between performance and increased oscillatory HPC-mPFC coupling (Jones and Wilson, 2005; Myroshnychenko et al., 2017; **Figure 9c**).

It is well established that the hippocampus is required for spatial tasks (Morris et al., 1982; O'Keefe and Nadel, 1978) and the same studies that associated the hippocampus with spatial navigation often also revealed the functions that do not depend on that area. Tasks requiring the animal to search for a reward based on a cue-guided or response strategy did not require a functioning hippocampus, further corroborating the notion that the hippocampus was especially important for allocentric navigation in space (Packard et al., 1989; Stringer et al., 2005). Despite the hippocampus' involvement in spatial processing, HPC cells showed similar phase locking strength to HPC theta in the spatial and light-guided task (**Figure 9d**). Finally, given the prominent role of the mPFC and hippocampus in rule-switching and spatial navigation, respectively, one might expect that during light-to-space rule switches the mPFC executes cognitive control over the hippocampus, and thereby engages it for the switch to the spatial strategy. However, measuring interregional communication with coherence and phase locking showed that coherence was similarly increased during post-switch blocks after a space-to-light and light-to-space rule switch (**Figure 8a,b**), as was mPFC phase locking strength during the two rules (**Figure 9d**).

A study training mice over four days to find an escape hole in the Barnes maze found increased HPC-mPFC coordination with spatial learning (Negrón-Oyarzo et al., 2018). Escape latency was large on the first day and gradually decreased, paralleled by a shift from a non-spatial strategy, involving visiting of all possible escape holes, to a spatial strategy, involving direct navigation to the escape hole. Slow gamma, but not theta, coherence increased over the four days and phase-locking strength of mPFC neurons to hippocampal theta, but not gamma, was increased for the spatial strategy. Recordings of the Negrón-Oyarzo et al. study were performed during learning of the task, whilst in our task the animal knew the procedure of the task and has experienced the light and spatial strategy at least once before. Therefore increased coordination between these two structures in the Negrón-Oyarzo et al. study might be more related to memory formation or retrieval on day

four. We also repeated our phase locking analysis on gamma band frequencies, however we did not find gamma coupling differences in the different maze parts or for the two rule types. Another study did however find increased hippocampal-mPFC theta coherence and mPFC phase locking on a spatial working memory task, compared to the cued version of the task (Hallock et al., 2016). This might be specific to the mPFC's involvement in working memory (Seamans et al., 1995).

Since we found increased HPC-mPFC theta coordination during all blocks and both rule types, the mPFC and hippocampus seem to engage during this task, irrespective of whether there was a recent rule switch or whether it is spatially- or cue-guided. Therefore, increased coordination seen in this task might be necessary for keeping the current rule online, or for maintaining goal-directed behavior. Also, it has been shown that when an animal is trained for both a spatially- and cue-guided task at the same time, the previously hippocampus-independent cue-guided task becomes hippocampus-dependent (Ferbinteanu, 2016). Therefore, in our study the hippocampus might cooperate with the striatal memory system during the light-guided rule.

Finally, we investigated the dynamics of mPFC phase locking to HPC theta during the pre-switch, switching and post-switch blocks. We found that the phase locking strength of mPFC cells changed throughout these blocks (**Figure 10**). But phase locking strength also changed between the first and second half of the stable rule 1 (remote recall) block, indicating that mPFC does not code for rule via phase locking and rather dynamically changes its locking to HPC theta over trials. Other studies have also highlighted the fact that mPFC population activity systematically shifts with time and persistently changes irrespective of learning (Hyman et al., 2012; Singh et al., 2019).

Rule remapping

Previous studies demonstrated neural population activity changes in the mPFC during rule-switching tasks (Durstewitz et al., 2010; Guise and Shapiro, 2017; Karlsson et al., 2012; Powell and Redish, 2016). It has therefore been suggested that the mPFC either codes for task rules or the insight that the behavioral strategy needs to be adapted. We performed cofiring and rate map correlations, but did not detect a consistent switching-associated shift in mPFC activity (**Figure 12-14**). With reference to other studies the following discusses

possible explanations why such a rule-switching-related shift in mPFC activity was not conclusively found in our data.

The Durstewitz et al. study involved an operant chamber task where the animal had to switch from a cue- to response-guided rule. This study found that not only could the rule be predicted from the firing rates of the mPFC population, but that an abrupt network transition occurred during the rule-switching period. Due to reports that with increasing rule familiarity the mPFC becomes less involved (Rich and Shapiro, 2007), recordings in their study were performed on rats that had never experienced the response-guided rule before. It is possible that mPFC network responses are more pronounced when the rule is completely novel, implicating the mPFC in learning. However, when they predicted the choice with mPFC population firing rates, the authors only selected so-called conflict trials, e.g., when the rat had to press the left lever according to the response-rule but the visual cue would have indicated the right lever. Due to their task design this meant that two different behavioral responses were compared, the right-lever response before the switch and the left-lever response after the switch. Any differences in neural population found could be attributable to behavioral differences and not internal shifts in strategy. Additionally, choice prediction was significantly higher than chance for only 7 out of 13 sessions. Finally, the Durstewitz et al. study reported that there were distinct points in the population firing time series that showed fluctuations beyond the drifts observed elsewhere during the time series. That this network disruption was also only observed for 5 out of 13 sessions, indicates that the neural subpopulation recorded from likely determines whether rule-switching related neural network changes in the mPFC are observed. Future analysis of the present data should therefore test for rule-related changes in the mPFC separately for every session, since a different neural population was recorded for every session.

The Karlsson et al. study employed an operant lever task where one of two tones signaled reward in the high or low probability port. An uncued change in outcome probability for the ports is then introduced. Since reward outcome of the ports fluctuated before the rule switch, it took many trials until the rat accumulated enough evidence and recognized a rule change. This study reported a pronounced increase in population firing rate variability (over ten trials), that was not associated with improved performance, but instead the realization that the rule had changed and alternative strategies had to be explored. We too tested for increased firing rate variability in the mPFC (not included in the Results of this thesis) and did observe abrupt increases in variability after introducing the rule switch, but only in a

subset of sessions. Keeping in mind that also the Durstewitz et al. study saw their rule switch-related changes only in a subset of their data suggests that we perhaps too should focus and perform more analysis on those sessions where an increased network firing variability was observed. In the Karlsson et al. study the rat had to accumulate evidence over many trials to recognize a rule change, whilst in the present study a rule change can be noticed after the first trial. A sustained attentional demand over many trials might be reflected in more pronounced mPFC network activity changes. Finally, their study recorded from AC neurons.

The Guise and Shapiro study, similar to us, used a plus-maze rule-switching task and recorded unit activity from the mPFC and hippocampus. However, differently to us, animals had to perform an intradimensional switch between two spatial rules (go-east and go-west). The two rules in their task therefore never involved the same trajectory (see Methods - Trajectories). To compare identical spatial behaviors the authors only analyzed neural activity in the start arm and reported that the ensemble activity in the mPFC and hippocampus distinguished between rules. One potential confound with their finding, however, is that both the mPFC and hippocampus, exhibit trajectory-specific firing (Ito et al., 2015; Wood et al., 2000). Therefore, although the neural activity of the first and second rule was compared during the same behavior (i.e., during the start arm), “rule-coding” might have only been observed because neural populations show differences in firing rate on the same start arm, depending on whether the animal will do a south-to-east or south-to-west trajectory. Another explanation for the discrepancy between the Guise and Shapiro and our study is the recorded neural population. Whilst we recorded from dorsal Prl, the Guise and Shapiro study recorded from ventral Prl and Ifl.

When analyzing changes in mPFC activity in relation to rule-switching it is important to be aware that mPFC network activity has been reported to systematically shift with time (Hyman et al., 2012). Analyzing mPFC population activity in the sleep before and after a Y-maze task, showed that excitability of the mPFC population always changed, irrespective of whether a new rule has been learnt (Singh et al., 2019). Therefore, changes of mPFC firing may code for the time spent on the task and can wrongly be associated with rule coding. The difference between learning and non-learning on the Y-maze task was that firing rate changes occurring during the task were carried over to subsequent sleep only when the animal learnt (Singh et al., 2019).

Trajectory replay

We confirmed previous studies and found that the mPFC displays spatially selective firing (Fujisawa et al., 2008; Hok et al., 2013; Zielinski et al., 2019). However, instead of coding for specific locations by distinguishing between the two start and goal arms, mPFC activity encoded the relative position between the start and the goal (**Figure 16b**). The mPFC might, therefore, have a role in the generalization of places with similar meaning (Yu et al., 2018). In the plus-maze, this generalization might allow the mPFC to code for the overarching task rule, i.e., run down the start arm and then choose one of the two goal arms.

We further demonstrated that non-local activity in the mPFC during immobility can be temporally-organized and represent entire spatial trajectories that extend in front or behind of the animal's current location. Replay of behaviorally-driven firing sequences has previously been demonstrated for the mPFC during sleep, however the content of what was being replayed was not investigated (Euston et al., 2007). The finding that the mPFC can replay sequences with a behavioral significance makes it more likely that mPFC replay has a behavioral function. In addition, since mPFC trajectory replay does not only progress in the forward, but also in the backward order (**Figure 19c,d**), it is not a mere reiteration, but an abstraction from the original experience. Furthermore, the relationship of mPFC trajectory replay at the goal with rule-switching performance and its increased occurrence during error trials, suggests that the ability to switch rules might, at least in part, underlie temporally-organized replay in the mPFC.

What might be the role of mPFC trajectory replay during awake immobility? To address this question one has to keep in mind that, according to our data, the mPFC retains only part of the spatial information found in HPC representations: it generates a trajectory-independent representation by generalizing between the two start and two goal arms. The fundamental elements comprising the task entail running down a start arm and, at the maze center, choosing one of the goal arms. An understanding of these fundamental task elements does not necessitate differentiation of the two start and goal arms, and therefore, the mPFC might, in fact, code for the overall structure of the task. It has previously been shown that the mPFC holds the neurobiological basis of schemas, which are higher-level frameworks of knowledge onto which new related information can rapidly be assimilated (Tse et al., 2011, 2007). In the present task, the overall task structure may be represented in the mPFC as a schema onto

which the new rule can be mapped. We found that center (ahead) and goal mPFC replay was increased on error trials and that mPFC replay at the goal positively correlated with rule-switching performance. During periods before the animal adapts to the new rule, replay of the general task structure during immobility might therefore aid the determination of the specific rule currently in place. Alternatively, mPFC trajectory replay may constitute a more general outcome evaluation in the presence of changed reward contingencies (Passecker et al., 2019). Previous studies showed that firing in the mPFC is modulated by errors and that anticipatory firing of this brain area decreases at reward absences, indicating an evaluative role for the mPFC (Narayanan and Laubach, 2008; Pratt and Mizumori, 2001; Sul et al., 2010).

Although replay in the hippocampus is being extensively studied, the functional relevance of hippocampal replay is not clear either. The behavioral state (i.e., sleep or awake) and cognitive demand likely determine the functional role of replay (Stella et al., 2019). Hippocampal replay during sleep is thought to underlie memory consolidation (Dupret et al., 2010; Girardeau et al., 2009; Wilson and McNaughton, 1994), whereas awake replay has been suggested to support planning of future paths (Pfeiffer and Foster, 2013; Xu et al., 2019). At movement initiation and during goal-directed behavior, the hippocampus mostly replayed trajectories that were ahead of the animal (Diba and Buzsáki, 2007; Pfeiffer and Foster, 2013). Furthermore, in a circular track replayed trajectories during theta oscillations could predict the animal's next visited goal and reactivation during SWRs was increased preceding correct compared to incorrect trials (Singer et al., 2013; Wikenheiser and Redish, 2015). However, other studies demonstrated that awake replay in the hippocampus is not necessarily linked to ongoing behavior or reactivates trajectories that are avoided by the animal (Gupta et al., 2010; Wu et al., 2017). One explanation for the opposing findings might be that hippocampal awake replay has different roles, depending on the task demands. For example, trajectory replay during a reference memory task predicted the future choice, but replay in the working memory version of the same task predicted the past choice (Xu et al., 2019). A similar task-dependent function for mPFC replay may also exist.

Our data suggests that HPC and mPFC trajectory replay in this task serve different functions. We found that trajectory replay in the HPC and mPFC do not co-occur and are oppositely correlated to rule-switching performance. Moreover, HPC replay in the center (both ahead and behind) is decreased on error trials, whilst (ahead) mPFC trajectory replay at the center is increased. That trajectory replay events in these two areas seemed to not

co-occur was unexpected since mPFC replay, so far, was mostly studied in temporal-alignment with hippocampal SWRs or hippocampal replay (Jadhav et al., 2016; Peyrache et al., 2009; Tang et al., 2017; Yu et al., 2018). In this task HPC replay might thereby rather support plus-maze task performance when the rule is stable (Ferbinteanu, 2016), whereas replay in the mPFC might be important when the rule has changed and a shift of strategy is required.

That replay of trajectories has not been discovered in the mPFC before could be explained with several reasons. First, without the 1D decoding used here, decoding precision would be low and therefore also the number of sequential and smooth trajectory replay events. Additionally, by increasing the number of tetrodes targeting the mPFC, the activity of a larger population of mPFC cells could be recorded, and hence more continuous events detected. Finally, it is possible that by using a task that depends on mPFC function the likelihood of detecting trajectory replay events in the mPFC is higher.

In summary, the presence of sequential reactivation of locations in the mPFC during the awake state and their relevance to rule-switching performance indicate that temporally-organized replay is a neural computation mechanism common to different brain areas (Ji and Wilson, 2007; Ólafsdóttir et al., 2016; O'Neill et al., 2017). With the discovery that hippocampal replay can be organized, new avenues opened in which hippocampal mnemonic computations could be analyzed. Similarly, the discovery of awake trajectory replay in the mPFC and their relevance to the performance of rule-switching offers new ways in which mPFC function can be investigated.

REFERENCES

Ambrose, R.E., Pfeiffer, B.E., Foster, D.J., 2016. Reverse replay of hippocampal place cells is uniquely modulated by changing reward. Neuron 91, 1124–1136. https://doi.org/10.1016/j.neuron.2016.07.047

Andersen, P., 1975. Organization of hippocampal neurons and their interconnections, in: Isaacson, R.L., Pribram, K.H. (Eds.), The Hippocampus: Volume 1: Structure and Development. Springer US, Boston, MA, pp. 155–175. https://doi.org/10.1007/978-1-4684-2976-3_7

Asaad, W.F., Eskandar, E.N., 2011. Encoding of both positive and negative reward prediction errors by neurons of the primate lateral prefrontal cortex and caudate nucleus. J. Neurosci. 31, 17772–17787. https://doi.org/10.1523/JNEUROSCI.3793-11.2011

Averbeck, B.B., Latham, P.E., Pouget, A., 2006. Neural correlations, population coding and computation. Nat. Rev. Neurosci. 7, 358–366. https://doi.org/10.1038/nrn1888

Baeg, E.H., Kim, Y.B., Huh, K., Mook-Jung, I., Kim, H.T., Jung, M.W., 2003. Dynamics of population code for working memory in the prefrontal cortex. Neuron 40, 177–188. https://doi.org/10.1016/S0896-6273(03)00597-X

Banerjee, A., Larsen, R.S., Philpot, B.D., Paulsen, O., 2016. Roles of presynaptic NMDA receptors in neurotransmission and plasticity. Trends Neurosci. 39, 26–39. https://doi.org/10.1016/j.tins.2015.11.001

Barker, G.R.I., Banks, P.J., Scott, H., Ralph, G.S., Mitrophanous, K.A., Wong, L.-F., Bashir, Z.I., Uney, J.B., Warburton, E.C., 2017. Separate elements of episodic memory subserved by distinct hippocampal–prefrontal connections. Nat. Neurosci. 20, 242–250. https://doi.org/10.1038/nn.4472

Benchenane, K., Peyrache, A., Khamassi, M., Tierney, P.L., Gioanni, Y., Battaglia, F.P., Wiener, S.I., 2010. Coherent theta oscillations and reorganization of spike timing in the hippocampal- prefrontal network upon learning. Neuron 66, 921–936. https://doi.org/10.1016/j.neuron.2010.05.013

Birrell, J.M., Brown, V.J., 2000. Medial frontal cortex mediates perceptual attentional set shifting in the rat. J. Neurosci. 20, 4320–4324. https://doi.org/10.1523/JNEUROSCI.20-11-04320.2000

Bissonette, G.B., Roesch, M.R., 2015. Neural correlates of rules and conflict in medial prefrontal cortex during decision and feedback epochs. Front. Behav. Neurosci. 9, 266. https://doi.org/10.3389/fnbeh.2015.00266

Buzsáki, G., Draguhn, A., 2004. Neuronal oscillations in cortical networks. Science 304, 1926–1929. https://doi.org/10.1126/science.1099745

Buzsaki, G., Horvath, Z., Urioste, R., Hetke, J., Wise, K., 1992. High-frequency network oscillation in the hippocampus. Science 256, 1025–1027. https://doi.org/10.1126/science.1589772

Cheng, S., Frank, L.M., 2008. New experiences enhance coordinated neural activity in the hippocampus. Neuron 57, 303–313. https://doi.org/10.1016/j.neuron.2007.11.035

Colombo, P.J., Brightwell, J.J., Countryman, R.A., 2003. Cognitive strategy-specific increases in phosphorylated cAMP response element-binding protein and c-Fos in the hippocampus and dorsal striatum. J. Neurosci. 23, 3547–3554.

Csicsvari, J., Hirase, H., Czurko, A., Buzsáki, G., 1998. Reliability and state dependence of pyramidal cell–interneuron synapses in the hippocampus: an ensemble approach in the behaving rat. Neuron 21, 179–189. https://doi.org/10.1016/S0896-6273(00)80525-5

Csicsvari, J., Hirase, H., Czurkó, A., Mamiya, A., Buzsáki, G., 1999. Fast network oscillations in the hippocampal CA1 region of the behaving rat. J. Neurosci. 19, RC20.
Csicsvari, J., O'Neill, J., Allen, K., Senior, T., 2007. Place-selective firing contributes to the reverse-order reactivation of CA1 pyramidal cells during sharp waves in open-field exploration. Eur. J. Neurosci. 26, 704–716. https://doi.org/10.1111/j.1460-9568.2007.05684.x
Davidson, T.J., Kloosterman, F., Wilson, M.A., 2009. Hippocampal replay of extended experience. Neuron 63, 497–507. https://doi.org/10.1016/j.neuron.2009.07.027
de Bruin, J.P.C., Sa`nchez-Santed, F., Heinsbroek, R.P.W., Donker, A., Postmes, P., 1994. A behavioural analysis of rats with damage to the medial prefrontal cortex using the morris water maze: evidence for behavioural flexibility, but not for impaired spatial navigation. Brain Res. 652, 323–333. https://doi.org/10.1016/0006-8993(94)90243-7
Delatour, B., Witter, M.P., 2002. Projections from the parahippocampal region to the prefrontal cortex in the rat: evidence of multiple pathways. Eur. J. Neurosci. 15, 1400–1407. https://doi.org/10.1046/j.1460-9568.2002.01973.x
Diba, K., Buzsáki, G., 2007. Forward and reverse hippocampal place-cell sequences during ripples. Nat. Neurosci. 10, 1241–1242. https://doi.org/10.1038/nn1961
Dragoi, G., Tonegawa, S., 2011. Preplay of future place cell sequences by hippocampal cellular assemblies. Nature 469, 397–401. https://doi.org/10.1038/nature09633
Dupret, D., O'Neill, J., Pleydell-Bouverie, B., Csicsvari, J., 2010. The reorganization and reactivation of hippocampal maps predict spatial memory performance. Nat. Neurosci. 13, 995–1002. https://doi.org/10.1038/nn.2599
Durstewitz, D., Vittoz, N.M., Floresco, S.B., Seamans, J.K., 2010. Abrupt transitions between prefrontal neural ensemble states accompany behavioral transitions during rule learning. Neuron 66, 438–448. https://doi.org/10.1016/j.neuron.2010.03.029
Ego-Stengel, V., Wilson, M.A., 2010. Disruption of ripple-associated hippocampal activity during rest impairs spatial learning in the rat. Hippocampus 20, 1–10. https://doi.org/10.1002/hipo.20707
Eichenbaum, H., 2001. The hippocampus and declarative memory: cognitive mechanisms and neural codes. Behav. Brain Res. 127, 199–207. https://doi.org/10.1016/S0166-4328(01)00365-5
Euston, D.R., Tatsuno, M., McNaughton, B.L., 2007. Fast-forward playback of recent memory sequences in prefrontal cortex during sleep. Science 318, 1147–1150. https://doi.org/10.1126/science.1148979
Ferbinteanu, J., 2016. Contributions of hippocampus and striatum to memory-guided behavior depend on past experience. J. Neurosci. 36, 6459–6470. https://doi.org/10.1523/JNEUROSCI.0840-16.2016
Floresco, S.B., Seamans, J.K., Phillips, A.G., 1997. Selective roles for hippocampal, prefrontal cortical, and ventral striatal circuits in radial-arm maze tasks with or without a delay. J. Neurosci. 17, 1880–1890. https://doi.org/10.1523/JNEUROSCI.17-05-01880.1997
Foster, D.J., Wilson, M.A., 2006. Reverse replay of behavioural sequences in hippocampal place cells during the awake state. Nature 440, 680–683. https://doi.org/10.1038/nature04587
Fries, P., 2005. A mechanism for cognitive dynamics: neuronal communication through neuronal coherence. Trends Cogn. Sci. 9, 474–480. https://doi.org/10.1016/j.tics.2005.08.011
Fujisawa, S., Amarasingham, A., Harrison, M.T., Buzsáki, G., 2008. Behavior-dependent short-term assembly dynamics in the medial prefrontal cortex. Nat. Neurosci. 11, 823–833. https://doi.org/10.1038/nn.2134
Gan, J., Weng, S., Pernía-Andrade, A.J., Csicsvari, J., Jonas, P., 2017. Phase-locked

inhibition, but not excitation, underlies hippocampal ripple oscillations in awake mice in vivo. Neuron 93, 308–314. https://doi.org/10.1016/j.neuron.2016.12.018
Girardeau, G., Benchenane, K., Wiener, S.I., Buzsáki, G., Zugaro, M.B., 2009. Selective suppression of hippocampal ripples impairs spatial memory. Nat. Neurosci. 12, 1222–1223. https://doi.org/10.1038/nn.2384
Grosmark, A.D., Buzsáki, G., 2016. Diversity in neural firing dynamics supports both rigid and learned hippocampal sequences. Science 351, 1440–1443. https://doi.org/10.1126/science.aad1935
Guise, K.G., Shapiro, M.L., 2017. Medial prefrontal cortex reduces memory interference by modifying hippocampal encoding. Neuron 94, 183-192.e8. https://doi.org/10.1016/j.neuron.2017.03.011
Gupta, A.S., van der Meer, M.A.A., Touretzky, D.S., Redish, A.D., 2010. Hippocampal replay is not a simple function of experience. Neuron 65, 695–705. https://doi.org/10.1016/j.neuron.2010.01.034
Hallock, H.L., Wang, A., Griffin, A.L., 2016. Ventral midline thalamus is critical for hippocampal–prefrontal synchrony and spatial working memory. J. Neurosci. 36, 8372–8389. https://doi.org/10.1523/JNEUROSCI.0991-16.2016
Harris, K.D., Henze, D.A., Csicsvari, J., Hirase, H., Buzsáki, G., 2000. Accuracy of tetrode spike separation as determined by simultaneous intracellular and extracellular measurements. J. Neurophysiol. 84, 401–414. https://doi.org/10.1152/jn.2000.84.1.401
Heidbreder, C.A., Groenewegen, H.J., 2003. The medial prefrontal cortex in the rat: evidence for a dorso-ventral distinction based upon functional and anatomical characteristics. Neurosci. Biobehav. Rev. 27, 555–579. https://doi.org/10.1016/j.neubiorev.2003.09.003
Hok, V., Chah, E., Save, E., Poucet, B., 2013. Prefrontal cortex focally modulates hippocampal place cell firing patterns. J. Neurosci. 33, 3443–3451. https://doi.org/10.1523/JNEUROSCI.3427-12.2013
Hok, V., Save, E., Lenck-Santini, P.P., Poucet, B., 2005. Coding for spatial goals in the prelimbic/infralimbic area of the rat frontal cortex. Proc. Natl. Acad. Sci. 102, 4602–4607. https://doi.org/10.1073/pnas.0407332102
Hoover, W.B., Vertes, R.P., 2007. Anatomical analysis of afferent projections to the medial prefrontal cortex in the rat. Brain Struct. Funct. 212, 149–179. https://doi.org/10.1007/s00429-007-0150-4
Huxter, J.R., Senior, T.J., Allen, K., Csicsvari, J., 2008. Theta phase–specific codes for two-dimensional position, trajectory and heading in the hippocampus. Nat. Neurosci. 11, 587–594. https://doi.org/10.1038/nn.2106
Hyman, J.M., Ma, L., Balaguer-Ballester, E., Durstewitz, D., Seamans, J.K., 2012. Contextual encoding by ensembles of medial prefrontal cortex neurons. Proc. Natl. Acad. Sci. 109, 5086–5091. https://doi.org/10.1073/pnas.1114415109
Ito, H.T., Zhang, S.-J., Witter, M.P., Moser, E.I., Moser, M.-B., 2015. A prefrontal–thalamo–hippocampal circuit for goal-directed spatial navigation. Nature 522, 50–55. https://doi.org/10.1038/nature14396
Jadhav, S.P., Kemere, C., German, P.W., Frank, L.M., 2012. Awake hippocampal sharp-wave ripples support spatial memory. Science 336, 1454–1458. https://doi.org/10.1126/science.1217230
Jadhav, S.P., Rothschild, G., Roumis, D.K., Frank, L.M., 2016. Coordinated excitation and inhibition of prefrontal ensembles during awake hippocampal sharp-wave ripple events. Neuron 90, 113–127. https://doi.org/10.1016/j.neuron.2016.02.010
Ji, D., Wilson, M.A., 2007. Coordinated memory replay in the visual cortex and hippocampus during sleep. Nat. Neurosci. 10, 100–107. https://doi.org/10.1038/nn1825

Jones, M.W., Wilson, M.A., 2005. Theta rhythms coordinate hippocampal–prefrontal interactions in a spatial memory task. PLOS Biol. 3, e402. https://doi.org/10.1371/journal.pbio.0030402
Jung, M.W., Qin, Y., McNaughton, B.L., Barnes, C., 1998. Firing characteristics of deep layer neurons in prefrontal cortex in rats performing spatial working memory tasks. Cereb. Cortex 8, 437–450. http://dx.doi.org/10.1093/cercor/8.5.437
Kaefer, K., Malagon-Vina, H., Dickerson, D.D., O'Neill, J., Trossbach, S.V., Korth, C., Csicsvari, J., 2019. Disrupted-in-schizophrenia 1 overexpression disrupts hippocampal coding and oscillatory synchronization. Hippocampus. https://doi.org/10.1002/hipo.23076
Karlsson, M.P., Tervo, D.G.R., Karpova, A.Y., 2012. Network resets in medial prefrontal cortex mark the onset of behavioral uncertainty. Science 338, 135–139. https://doi.org/10.1126/science.1226518
Kyd, R.J., Bilkey, D.K., 2003. Prefrontal cortex lesions modify the spatial properties of hippocampal place cells. Cereb. Cortex 13, 444–451. https://doi.org/10.1093/cercor/13.5.444
Leutgeb, S., Leutgeb, J.K., Barnes, C.A., Moser, E.I., McNaughton, B.L., Moser, M.-B., 2005. Independent codes for spatial and episodic memory in hippocampal neuronal ensembles. Science 309, 619–623. https://doi.org/10.1126/science.1114037
Lever, C., Burton, S., Jeewajee, A., Wills, T.J., Cacucci, F., Burgess, N., O'Keefe, J., 2010. Environmental novelty elicits a later theta phase of firing in CA1 but not subiculum. Hippocampus 20, 229–234. https://doi.org/10.1002/hipo.20671
Louie, K., Wilson, M.A., 2001. Temporally structured replay of awake hippocampal ensemble activity during rapid eye movement sleep. Neuron 29, 145–156. https://doi.org/10.1016/S0896-6273(01)00186-6
Lüscher, C., Malenka, R.C., 2012. NMDA receptor-dependent long-term potentiation and long-term depression (LTP/LTD). Cold Spring Harb. Perspect. Biol. 4. https://doi.org/10.1101/cshperspect.a005710
Maingret, N., Girardeau, G., Todorova, R., Goutierre, M., Zugaro, M., 2016. Hippocampo-cortical coupling mediates memory consolidation during sleep. Nat. Neurosci. 19, 959–964. https://doi.org/10.1038/nn.4304
Markus, E.J., Qin, Y.L., Leonard, B., Skaggs, W.E., McNaughton, B.L., Barnes, C.A., 1995. Interactions between location and task affect the spatial and directional firing of hippocampal neurons. J. Neurosci. 15, 7079–7094. https://doi.org/10.1523/JNEUROSCI.15-11-07079.1995
McKlveen, J.M., Myers, B., Herman, J.P., 2015. The medial prefrontal cortex: coordinator of autonomic, neuroendocrine and behavioural responses to stress. J. Neuroendocrinol. 27, 446–456. https://doi.org/10.1111/jne.12272
Milner, B., 1963. Effects of different brain lesions on card sorting: The role of the frontal lobes. Arch. Neurol. 9, 90–100. https://doi.org/10.1001/archneur.1963.00460070100010
Morris, R.G., Garrud, P., Rawlins, J.N., O'Keefe, J., 1982. Place navigation impaired in rats with hippocampal lesions. Nature 297, 681–683. https://doi.org/10.1038/297681a0
Muller, R.U., Kubie, J.L., 1987. The effects of changes in the environment on the spatial firing of hippocampal complex-spike cells. J. Neurosci. 7, 1951–1968. https://doi.org/10.1523/JNEUROSCI.07-07-01951.1987
Muller, R.U., Kubie, J.L., Ranck, J.B., 1987. Spatial firing patterns of hippocampal complex-spike cells in a fixed environment. J. Neurosci. 7, 1935–1950. https://doi.org/10.1523/JNEUROSCI.07-07-01935.1987
Myroshnychenko, M., Seamans, J.K., Phillips, A.G., Lapish, C.C., 2017. Temporal dynamics of hippocampal and medial prefrontal cortex interactions during the delay period of a

working memory-guided foraging task. Cereb. Cortex 27, 5331–5342. https://doi.org/10.1093/cercor/bhx184
Narayanan, N.S., Laubach, M., 2008. Neuronal correlates of post-error slowing in the rat dorsomedial prefrontal cortex. J. Neurophysiol. 100, 520–525. https://doi.org/10.1152/jn.00035.2008
Navawongse, R., Eichenbaum, H., 2013. Distinct pathways for rule-based retrieval and spatial mapping of memory representations in hippocampal neurons. J. Neurosci. 33, 1002–1013. https://doi.org/10.1523/JNEUROSCI.3891-12.2013
Negrón-Oyarzo, I., Espinosa, N., Aguilar-Rivera, M., Fuenzalida, M., Aboitiz, F., Fuentealba, P., 2018. Coordinated prefrontal–hippocampal activity and navigation strategy-related prefrontal firing during spatial memory formation. Proc. Natl. Acad. Sci. 115, 7123–7128. https://doi.org/10.1073/pnas.1720117115
O'Keefe, J., Dostrovsky, J., 1971. The hippocampus as a spatial map. Preliminary evidence from unit activity in the freely-moving rat. Brain Res. 34, 171–175. https://doi.org/10.1016/0006-8993(71)90358-1
O'Keefe, J., Nadel, L., 1978. The hippocampus as a cognitive map. Clarendon Press ; Oxford University Press, Oxford : New York.
O'Keefe, J., Recce, M.L., 1993. Phase relationship between hippocampal place units and the EEG theta rhythm. Hippocampus 3, 317–330. https://doi.org/10.1002/hipo.450030307
Ólafsdóttir, H.F., Carpenter, F., Barry, C., 2016. Coordinated grid and place cell replay during rest. Nat. Neurosci. 19, 792–794. https://doi.org/10.1038/nn.4291
O'Neill, J., Boccara, C.N., Stella, F., Schoenenberger, P., Csicsvari, J., 2017. Superficial layers of the medial entorhinal cortex replay independently of the hippocampus. Science 355, 184–188. https://doi.org/10.1126/science.aag2787
O'Neill, J., Senior, T., Csicsvari, J., 2006. Place-selective firing of CA1 pyramidal cells during sharp wave/ripple network patterns in exploratory behavior. Neuron 49, 143–155. https://doi.org/10.1016/j.neuron.2005.10.037
O'Neill, J., Senior, T.J., Allen, K., Huxter, J.R., Csicsvari, J., 2008. Reactivation of experience-dependent cell assembly patterns in the hippocampus. Nat. Neurosci. 11, 209–215. https://doi.org/10.1038/nn2037
Packard, M.G., Hirsh, R., White, N.M., 1989. Differential effects of fornix and caudate nucleus lesions on two radial maze tasks: evidence for multiple memory systems. J. Neurosci. 9, 1465–1472. https://doi.org/10.1523/JNEUROSCI.09-05-01465.1989
Passecker, J., Mikus, N., Malagon-Vina, H., Anner, P., Dimidschstein, J., Fishell, G., Dorffner, G., Klausberger, T., 2019. Activity of prefrontal neurons predict future choices during gambling. Neuron 101, 152-164.e7. https://doi.org/10.1016/j.neuron.2018.10.050
Pavlides, C., Winson, J., 1989. Influences of hippocampal place cell firing in the awake state on the activity of these cells during subsequent sleep episodes. J. Neurosci. 9, 2907–2918. https://doi.org/10.1523/JNEUROSCI.09-08-02907.1989
Peyrache, A., Khamassi, M., Benchenane, K., Wiener, S.I., Battaglia, F.P., 2009. Replay of rule-learning related neural patterns in the prefrontal cortex during sleep. Nat. Neurosci. 12, 919–926. https://doi.org/10.1038/nn.2337
Pfeiffer, B.E., Foster, D.J., 2013. Hippocampal place-cell sequences depict future paths to remembered goals. Nature 497, 74–79. https://doi.org/10.1038/nature12112
Place, R., Farovik, A., Brockmann, M., Eichenbaum, H., 2016. Bidirectional prefrontal-hippocampal interactions support context-guided memory. Nat. Neurosci. 19, 992–994. https://doi.org/10.1038/nn.4327
Powell, N.J., Redish, A.D., 2016. Representational changes of latent strategies in rat medial prefrontal cortex precede changes in behaviour. Nat. Commun. 7, 12830.

https://doi.org/10.1038/ncomms12830
Pratt, W.E., Mizumori, S.J.Y., 2001. Neurons in rat medial prefrontal cortex show anticipatory rate changes to predictable differential rewards in a spatial memory task. Behav. Brain Res. 123, 165–183. https://doi.org/10.1016/S0166-4328(01)00204-2
Ragozzino, M.E., Detrick, S., Kesner, R.P., 1999a. Involvement of the prelimbic–infralimbic areas of the rodent prefrontal cortex in behavioral flexibility for place and response learning. J. Neurosci. 19, 4585–4594. https://doi.org/10.1523/JNEUROSCI.19-11-04585.1999
Ragozzino, M.E., Wilcox, C., Raso, M., Kesner, R.P., 1999b. Involvement of rodent prefrontal cortex subregions in strategy switching. Behav. Neurosci. 113, 32–41. https://doi.org/10.1037/0735-7044.113.1.32
Rich, E.L., Shapiro, M., 2009. Rat prefrontal cortical neurons selectively code strategy switches. J. Neurosci. 29, 7208–7219. https://doi.org/10.1523/JNEUROSCI.6068-08.2009
Rich, E.L., Shapiro, M.L., 2007. Prelimbic/infralimbic inactivation impairs memory for multiple task switches, but not flexible selection of familiar tasks. J. Neurosci. 27, 4747–4755. https://doi.org/10.1523/JNEUROSCI.0369-07.2007
Rolls, E., Treves, A., 1998. Neural networks and brain function. Oxford University Press, Oxford.
Scoville, W.B., Milner, B., 1957. Loss of recent memory after bilateral hippocampal lesions. J. Neurol. Neurosurg. Psychiatry 20, 11–21.
Seamans, J.K., Floresco, S.B., Phillips, A.G., 1995. Functional differences between the prelimbic and anterior cingulate regions of the rat prefrontal cortex. Behav. Neurosci. 109, 1063–1073.
Siapas, A.G., Lubenov, E.V., Wilson, M.A., 2005. Prefrontal phase locking to hippocampal theta oscillations. Neuron 46, 141–151. https://doi.org/10.1016/j.neuron.2005.02.028
Silva, D., Feng, T., Foster, D.J., 2015. Trajectory events across hippocampal place cells require previous experience. Nat. Neurosci. 18, 1772–1779. https://doi.org/10.1038/nn.4151
Singer, A.C., Carr, M.F., Karlsson, M.P., Frank, L.M., 2013. Hippocampal SWR activity predicts correct decisions during the initial learning of an alternation task. Neuron 77, 1163–1173. https://doi.org/10.1016/j.neuron.2013.01.027
Singer, A.C., Frank, L.M., 2009. Rewarded outcomes enhance reactivation of experience in the hippocampus. Neuron 64, 910–921. https://doi.org/10.1016/j.neuron.2009.11.016
Singh, A., Peyrache, A., Humphries, M.D., 2019. Medial prefrontal cortex population activity is plastic irrespective of learning. J. Neurosci. 1370–17. https://doi.org/10.1523/JNEUROSCI.1370-17.2019
Skaggs, W.E., McNaughton, B.L., 1996. Replay of neuronal firing sequences in rat hippocampus during sleep following spatial experience. Science 271, 1870–1873. https://doi.org/10.1126/science.271.5257.1870
Spellman, T., Rigotti, M., Ahmari, S.E., Fusi, S., Gogos, J.A., Gordon, J.A., 2015. Hippocampal–prefrontal input supports spatial encoding in working memory. Nature 522, 309–314. https://doi.org/10.1038/nature14445
Stella, F., Baracskay, P., O'Neill, J., Csicsvari, J., 2019. Hippocampal reactivation of random trajectories resembling Brownian diffusion. Neuron. https://doi.org/10.1016/j.neuron.2019.01.052
Stringer, K.G., Martin, G.M., Skinner, D.M., 2005. The effects of hippocampal lesions on response, direction, and place learning in rats. Behav. Neurosci. 119, 946–952. https://doi.org/10.1037/0735-7044.119.4.946
Sul, J.H., Kim, H., Huh, N., Lee, D., Jung, M.W., 2010. Distinct roles of rodent orbitofrontal and medial prefrontal cortex in decision making. Neuron 66, 449–460.

https://doi.org/10.1016/j.neuron.2010.03.033
Tang, W., Shin, J.D., Frank, L.M., Jadhav, S.P., 2017. Hippocampal-prefrontal reactivation during learning is stronger in awake compared with sleep states. J. Neurosci. 37, 11789–11805. https://doi.org/10.1523/JNEUROSCI.2291-17.2017
Tolman, E.C., 1948. Cognitive maps in rats and men. Psychol. Rev. 55, 189–208. https://doi.org/10.1037/h0061626
Tse, D., Langston, R.F., Kakeyama, M., Bethus, I., Spooner, P.A., Wood, E.R., Witter, M.P., Morris, R.G.M., 2007. Schemas and memory consolidation. Science 316, 76–82. https://doi.org/10.1126/science.1135935
Tse, D., Takeuchi, T., Kakeyama, M., Kajii, Y., Okuno, H., Tohyama, C., Bito, H., Morris, R.G.M., 2011. Schema-dependent gene activation and memory encoding in neocortex. Science 333, 891–895. https://doi.org/10.1126/science.1205274
Uylings, H.B.M., Groenewegen, H.J., Kolb, B., 2003. Do rats have a prefrontal cortex? Behav. Brain Res., The Rodent Prefrontal Cortex 146, 3–17. https://doi.org/10.1016/j.bbr.2003.09.028
Vanderwolf, C.H., 1969. Hippocampal electrical activity and voluntary movement in the rat. Electroencephalogr. Clin. Neurophysiol. 26, 407–418.
Varela, C., Kumar, S., Yang, J.Y., Wilson, M.A., 2014. Anatomical substrates for direct interactions between hippocampus, medial prefrontal cortex, and the thalamic nucleus reuniens. Brain Struct. Funct. 219, 911–929. https://doi.org/10.1007/s00429-013-0543-5
Vertes, R.P., 2004. Differential projections of the infralimbic and prelimbic cortex in the rat. Synapse 51, 32–58. https://doi.org/10.1002/syn.10279
Vertes, R.P., Hoover, W.B., Do Valle, A.C., Sherman, A., Rodriguez, J. j., 2006. Efferent projections of reuniens and rhomboid nuclei of the thalamus in the rat. J. Comp. Neurol. 499, 768–796. https://doi.org/10.1002/cne.21135
Wierzynski, C.M., Lubenov, E.V., Gu, M., Siapas, A.G., 2009. State-dependent spike-timing relationships between hippocampal and prefrontal circuits during sleep. Neuron 61, 587–596. https://doi.org/10.1016/j.neuron.2009.01.011
Wilson, M.A., McNaughton, B.L., 1994. Reactivation of hippocampal ensemble memories during sleep. Science 265, 676–679. https://doi.org/10.1126/science.8036517
Wilson, M.A., McNaughton, B.L., 1993. Dynamics of the hippocampal ensemble code for space. Science 261, 1055–1058. https://doi.org/10.1126/science.8351520
Wood, E.R., Dudchenko, P.A., Robitsek, R.J., Eichenbaum, H., 2000. Hippocampal neurons encode information about different types of memory episodes occurring in the same location. Neuron 27, 623–633. https://doi.org/10.1016/S0896-6273(00)00071-4
Wu, C.-T., Haggerty, D., Kemere, C., Ji, D., 2017. Hippocampal awake replay in fear memory retrieval. Nat. Neurosci. 20, 571–580. https://doi.org/10.1038/nn.4507
Xu, H., Baracskay, P., O'Neill, J., Csicsvari, J., 2019. Assembly responses of hippocampal CA1 place cells predict learned behavior in goal-directed spatial tasks on the radial eight-arm maze. Neuron 101, 119-132.e4. https://doi.org/10.1016/j.neuron.2018.11.015
Xu, W., Südhof, T.C., 2013. A neural circuit for memory specificity and generalization. Science 339, 1290–1295. https://doi.org/10.1126/science.1229534
Ye, X., Kapeller-Libermann, D., Travaglia, A., Inda, M.C., Alberini, C.M., 2017. Direct dorsal hippocampal–prelimbic cortex connections strengthen fear memories. Nat. Neurosci. 20, 52–61. https://doi.org/10.1038/nn.4443
Yu, J.Y., Liu, D.F., Loback, A., Grossrubatscher, I., Frank, L.M., 2018. Specific hippocampal representations are linked to generalized cortical representations in memory. Nat. Commun. 9, 2209. https://doi.org/10.1038/s41467-018-04498-w
Zar, J.H., 2010. Biostatistical analysis, 5th ed. Prentice-Hall/Pearson, Upper Saddle River,

N.J.
Zhang, K., Ginzburg, I., McNaughton, B.L., Sejnowski, T.J., 1998. Interpreting neuronal population activity by reconstruction: unified framework with application to hippocampal place cells. J. Neurophysiol. 79, 1017–1044. https://doi.org/10.1152/jn.1998.79.2.1017
Zielinski, M.C., Shin, J.D., Jadhav, S.P., 2019. Coherent coding of spatial position mediated by theta oscillations in the hippocampus and prefrontal cortex. J. Neurosci. 0106–19. https://doi.org/10.1523/JNEUROSCI.0106-19.2019